Fall 2013

Libration point orbits near small bodies in the elliptic restricted three-body problem

Bharat Mahajan

Department:

LIBRATION POINT ORBITS NEAR SMALL BODIES

IN THE

ELLIPTIC RESTRICTED THREE-BODY PROBLEM

by

BHARAT MAHAJAN

A THESIS

Presented to the Faculty of the Graduate School of the

MISSOURI UNIVERSITY OF SCIENCE AND TECHNOLOGY

In Partial Fulfillment of the Requirements for the Degree

MASTER OF SCIENCE IN AEROSPACE ENGINEERING

2013

Approved by

Henry J. Pernicka, Co-Advisor
S. N. Balakrishnan, Co-Advisor
Joshua L. Rovey

ABSTRACT

In this study, the feasibility of using libration point orbits to explore small solar system bodies, including asteroids and comets, is considered. A novel design for a small body mission is proposed that makes use of libration point orbits as "parking" orbits. In considering a human exploration mission to asteroids or comets, these "parking" orbits may provide benefits including a safe vantage point for staging/observation, reduced perturbation effects from the nonuniform gravitational field of the body, fewer communication blackouts, ease of guidance and control of a lander on the surface, etc. Because small solar system bodies have extremely low mass ratios in the Sun-small body system, the existence of periodic orbits about the collinear libration points at a safe distance from the smaller primary was uncertain and is demonstrated for a range of small bodies. A two-level differential corrector along with periodicity constraints is proposed for use in computing periodic orbits in the vicinity of the small bodies with significant eccentricity in the Elliptic Restricted Three-Body Problem. Using this method, halo-like orbits are computed in the Sun-*433 Eros* and Sun-*4 Vesta* systems. The stability of these orbits is analyzed using Floquet theory. To overcome the effects of perturbations in these unstable orbits, a robust nonlinear station-keeping controller based on sliding mode control theory is proposed. The controller performance is validated in the presence of third-body perturbations from Jupiter, solar radiation pressure perturbations, tracking errors, orbit insertion errors and maneuver burn errors in the Sun-*433 Eros* and Sun-*4 Vesta* systems. Simulation results are presented that show that the small body missions can be designed using libration point orbits with feasible station-keeping costs.

ACKNOWLEDGMENTS

I would first like to thank my two co-advisers Dr. Hank Pernicka and Dr. S. N. Balakrishnan for guiding me patiently in my foray into the field of aerospace engineering. I feel truly lucky to have had the opportunity of working with them. My journey became a lot easier due to their support and latitude they allotted to me to pursue different problems as I please.

I also thank Dr. Joshua Rovey for his valuable time and effort in reviewing my thesis. I would also like to acknowledge his excellent teaching in the Plasma Physics class.

Additionally, I would like to thank the Missouri S&T Satellite team for giving me an opportunity for being a part of it. I would also like to thank the Department of Mechanical and Aerospace Engineering at Missouri S&T for providing me financial support in the form of teaching assistantship during my stay.

Last but definitely not the least, this work would not have been possible without encouragement and support from my parents and all my loved ones (too many names here!). They supported me in all the things that I wanted to do, however crazy they might sound like! I feel always protected by their unconditional love, no matter how far away they are…

TABLE OF CONTENTS

Page

LIST OF ILLUSTRATIONS

Page

LIST OF TABLES

Page

1. INTRODUCTION

1.1. MISSION TO SMALL BODIES

The Augustine Committee [1] recommendations suggest that human missions be considered involving the exploration of small solar system bodies including asteroids and comets. These small solar system bodies are "left-overs" of the solar system and hold a key to understanding its origin and how it evolved into its current state. The exact definition of a small solar system body is provided by the Resolution B5[1] (2006) of the International Astronomical Union, according to which all objects orbiting the Sun except the eight planets, dwarf planets such as Pluto and satellites, are small solar system bodies (SSSB). The list currently includes asteroids, comets, most Trans-Neptunian Objects and other small bodies. To date a few robotic missions have flown close to some SSSBs, and/or orbited these bodies, and in a few cases even landed on their surface.

Galileo was the first spacecraft to make a close-up study of the two asteroids *Gaspra* in 1991 and *Ida* in 1993. NEAR Shoemaker did a flyby of asteroid *253 Mathilde* in 1997 and orbited asteroid *433 Eros* in 2000. It provided very useful measurements of the mass, composition, size and shape information about *433 Eros*. It was also the first spacecraft to perform a controlled descent to its surface. Deep Space I spacecraft passed by the near-Earth asteroid *9669 Braille* on 28th July 1999 and encountered comet *Borrelly* on 22nd September 2001. Twelve new technologies were tested onboard Deep Space I including ion propulsion low-thrust technology, which made it the first interplanetary spacecraft to do so. The Stardust mission brought back samples of comet *Wild-2* during

[1] http://www.iau.org/static/resolutions/Resolution_GA26-5-6.pdf

its closest approach of 236 km to the comet. The Stardust mission was retargeted as Stardust NExT to encounter the comet *Tempel 1* in 2011. The comet *Tempel 1* was also visited by the Deep Impact spacecraft in 2005, which made use of an impactor to study the ejected debris. After the primary mission was completed, Deep Impact was retargeted as the EPOXI mission to encounter the *Hartley 2* comet and also to observe stars with known orbiting planets. Japan launched Hayabusa mission to collect the samples from the surface of asteroid *25143 Itokawa* in 2005. Hayabusa was the first spacecraft to land as well as to take off from the surface of an asteroid. Hayabusa also observed the asteroid surface by maintaining a position at a fixed distance from the asteroid in a close-by heliocentric orbit using station-keeping employing ion propulsion. European Space Agency's Rosetta mission was launched in 2004 and will be the first spacecraft to orbit and land on a comet *67P/Churyumov–Gerasimenko*. Dawn is a mission currently enroute to dwarf planet *1 Ceres* and orbited *4 Vesta* asteroid recently. It visited *4 Vesta* in 2011 and is destined to encounter *1 Ceres* in 2015. Two more missions are being planned to launch in future: Hayabusa 2 from Japan is designed to study asteroid *1999 JU3*. It has a lander and a rover and it aims to return samples its surface back to Earth. Similarly the OSIRIS-REx mission is currently under development to observe near-Earth asteroid *1999 RQ36* and bring back samples from its surface.

All the above missions observed the SSSB from a distance, performed a flyby or in a few cases orbited the SSSB and/or landed on its surface. In case of Hayabusa, the spacecraft surveyed the surface from a fixed distance of 20 km maintained by making use of active control applied using its ion engines. In contrast to the above missions, in this work a different mission design is proposed for SSSBs that makes use of libration point

orbits in their vicinity. The libration point orbits (LPOs) can be halo orbits, Lissajous orbits or planar Lyapunov orbits in the Sun-SSSB three-body restricted system with the SSSB orbiting around the Sun in an eccentric orbit. These LPOs can be used as "parking" orbits for a "mothership" spacecraft from which a lander, either robotic or human-operated, can detach itself and land on surface of the SSSB. Figure 1.1 shows an illustration (not to scale) of such a mission design where the Orion spacecraft acts as a "mothership" in an LPO in the Sun-*25143 Itokawa* system.

Most prior research identified in the literature is focused on understanding the dynamics in the immediate vicinity of SSSBs and design of transfer and landing trajectories. However the use of LPOs for facilitating missions to SSSBs has not yet received much attention. Using halo or similar LPOs for these missions may prove beneficial for a number of reasons including ability to provide an uninterrupted communication link from the surface of the small body to Earth and reduced nonuniform gravitational perturbation effects on the spacecraft in the LPO. Additionally it can provide a staging location safe from outgassing jets (for comets), and for observation and guidance and control of lander descent/ascent to/from the surface. The focus in this work is on the analysis of existence, stability and numerical computations of halo-like orbits for a range of small bodies in the Elliptic Restricted Three-Body Problem (ER3BP). Additionally, a robust nonlinear controller is designed to station-keep a spacecraft in the chosen reference LPO.

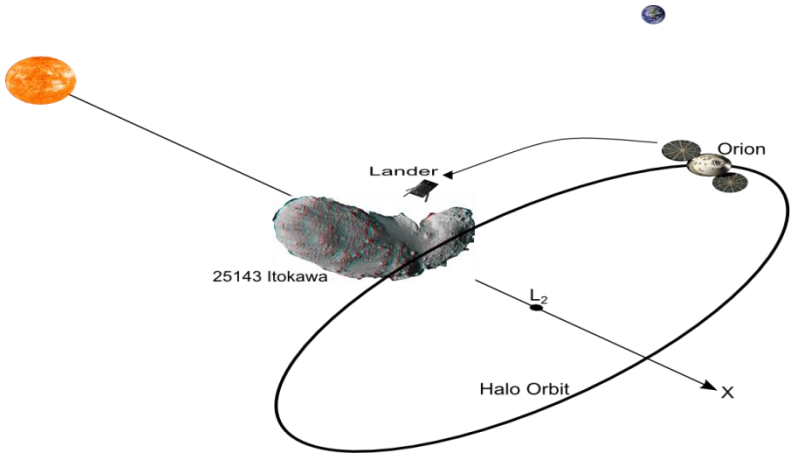

Figure 1.1. A Concept Mission Design Using Libration Point Orbits in the Sun-*25143 Itokawa* System (Figure not to Scale).

1.2. PROBLEM STATEMENT

This section states the questions and problem scenarios that set the direction and scope of this work. The assumptions made in simplifying the problem scenarios and the solutions sought are also stated.

1.2.1. Feasibility of LPOs Near Small Bodies. Most of the SSSBs have extremely small masses compared to the Sun and have much smaller mass ratios compared to the Earth-Moon and Sun-Earth systems. For instance, the mass ratio for Sun-*433 Eros* system is smaller than the Sun-Earth mass ratio by a magnitude of ninth order. The distance of the collinear libration point locations, L_1 and L_2, from the smaller primary is directly proportional to the mass ratio. To have a viable periodic orbit about these libration points, they must exist at an appropriately safe distance from the surface of the smaller primary. Additionally it is known that the three-dimensional halo periodic orbits have a minimum amplitude below which they do not exist. All these factors require

a thorough investigation of the existence of the collinear libration points and periodic orbits around them near SSSB.

1.2.2. Computation of LPOs Near Small Bodies. Almost all SSSBs exist in heliocentric orbits with significant eccentricity compared to the Earth's orbit. For instance, the eccentricity of *433 Eros* is 0.2229 whereas the eccentricity of the Earth's orbit is only 0.0167. Therefore it is imperative that a method is required to find periodic orbits in the Elliptic Restricted Three Body Problem with significant value of the eccentricity and small values of mass ratios. The chosen method should also be able to produce periodic orbits of different sizes and shapes that can fit the requirements of different types of missions. The computed solutions must be close to the actual dynamics, failing which might increase the station-keeping costs significantly.

1.2.3. Stability Analysis. The stability analysis of the computed LPOs near the SSSB provide important information about how fast the spacecraft will diverge from the chosen reference path due to the presence of various perturbations. This information can be useful for fine-tuning the station-keeping controllers.

1.2.4. Station-Keeping of the LPOs Near Small Bodies. In contrast to the major planetary bodies of the solar system, the information about SSSBs is limited in terms of physical and orbital properties. The lack of precise measurements of these bodies mass and locations necessitates the use of robust methods for station-keeping a spacecraft near these bodies. The station-keeping methods must be able to accommodate uncertainties in the dynamic model employed for computing the reference orbits and must be efficient in terms of the ΔV requirements. These methods should also be easily realizable using existing low-thrust propulsion technologies.

1.3. LITERATURE SURVEY

Leonard Euler was the first to define the restricted three-body problem in the eighteenth century and he also introduced the synodic coordinate system in connection to his lunar theories [2]. He is also credited with discovering the three collinear libration points. The triangular libration points were discovered by Lagrange and all the five equilibrium or libration points now bear his name [3]. These works were followed by the contributions in the nineteenth century by Jacobi, Hill and Poincaré. One of the most important contributions to the restricted three-body problem was the integral of motion found by Jacobi that bears his name. The Jacobian integral provided an important integral of motion for this dynamical system that helped in forming the qualitative behaviors of this problem. The application of this principle was used by Hill to show that the Earth-Moon distance must remain bounded from above for all time. The curves marking the boundary between forbidden and accessible regions in the restricted three-body problem computed using the Jacobian integral are today known as Hill's curves. Poincaré in 1899 provided important qualitative analysis of the celestial mechanics problem in general and also laid the foundation of chaos theory and topology [2]. In 1903, Plummer published a Fourier series solution for in-plane periodic orbits in the neighborhood of five libration points. He generalized the results already given by Darwin and Charlier and extended the analysis to second-order approximation for collinear libration points [4]. Moulton's school in 1920 pursued the quantitative approach and calculated many families of orbits in the restricted three-body problem. The classic text by Szebehely published in 1967 proved to be an essential reference on the research accomplished on restricted three-body problem by many researchers up to the 1960s [2]. While the main focus in this reference

was the Circular Restricted Three-Body Problem (CR3BP), a brief introduction to the ER3BP was also included.

Danby provided a linear stability analysis of the triangular libration points in the ER3BP [5]. Bennett used a similar approach and extended the stability analysis to also include collinear libration points. He showed that for the collinear libration points, there is no value of mass ratio and eccentricity for which variational stability exists [6]. Alfriend and Rand presented an analytic approach for determining the stability of infinitesimal motions about the triangular libration points in the ER3BP [7]. An analytic series solution for computing the characteristic exponents in the ER3BP is also given by Bennett [8]. Broucke presented a numerical method to compute planar periodic orbits in the ER3BP [9]. He used Moulton's criterion of strong periodicity to enforce perpendicular crossings at the syzygy axis when the primaries are at an apse. Broucke successfully calculated the in-plane Lyapunov orbits for all values of eccentricity and also computed the stability characteristics of these orbits in the ER3BP using Floquet analysis.

In the 1960s, the space race to reach the Moon attracted attention to the problem of lunar far-side communication. Various solutions had been proposed including placing a relay satellite at the L_2 libration point location. Schmid proposed a "Hummingbird" satellite anchored 65,000 km behind the Moon and perturbed by 300 km from the Earth-Moon L_2 libration point in the out-of-plane direction for maximum coverage [10]. An interesting concept of putting a lunar communication relay satellite in a three-dimensional periodic orbit about the Earth-Moon L_2 libration point was first proposed by Farquhar [11]. He coined the term "halo" orbit for these periodic orbits as these would

appear while encircling the Moon from behind when viewed from Earth. The Halo orbits had the advantage that a satellite in this orbit will be able to communicate to the lunar far side as well as to Earth without any interruptions. To find a halo orbit, the in-plane and out-of-plane motions about the collinear libration points must have a 1:1 resonance in their period. If this requirement is not met, the resulting quasi-periodic orbits appear as Lissajous figures from some viewpoints and are thus called Lissajous orbits. Farquhar and Kamel computed a third-order analytic solution for quasi-periodic libration point orbits in the Earth-Moon system [12]. The solution included lunar orbit eccentricity and the Sun's gravitational field. They used the Lindsedt-Poincaré method to show that for sufficiently large amplitudes, the nonlinear contributions make the in-plane and out-of-plane periods equal, thus establishing the existence of a three-dimensional periodic halo orbit. For the Earth-Moon system, they found the minimum in-plane amplitude as 32,379 km above which an out-of-plane amplitude can be found to make the two fundamental frequencies equal. Heppenheimer also computed a third-order solution for out-of-plane motion in the circular restricted problem for collinear as well as triangular points [13]. A generalized analytic third-order quasi-periodic solution for a satellite in the vicinity of L_1 and L_2 libration point locations is given by Richardson and Cary [14]. Their solution was based on the Sun-Earth-Moon CR3BP system with effects due to eccentricity of the Earth-Moon barycenter's heliocentric orbit and the Earth-Moon mass ratio included. Using a similar approach, Richardson presented a third-order analytic solution for periodic halo orbits in the CR3BP about the collinear libration points by using the Lindsedt-Poincaré method [15]. This analytic series solution is used in this work to compute the minimum size of halo orbits in the Sun-SSSB system.

Gomez *et al.* proposed quasi-halo orbits that are Lissajous orbits which maintain an exclusion zone for the out-of-plane motion similar to halo orbits [16]. They presented a semi-analytic approach to compute such orbits. Howell presented a numerical algorithm to compute periodic three-dimensional halo orbits in the vicinity of the collinear points in the CR3BP [17]. This method exploits the symmetry property of the halo orbits and uses differential corrections to enforce perpendicular crossings at the *x*-*z* plane. It was shown that the halo orbits can be computed for any value of mass ratio using this numerical method. A similar approach is used in this work to compute halo orbits near small bodies in the CR3BP. Howell also computed the stability of the halo orbits and found the range of mass ratios that produce stable halo orbits [17]. To compute the halo orbits numerically in the ER3BP, Howell used the approach proposed by Broucke [9] with Lyapunov orbits and extended it to compute three-dimensional halo orbits for systems with mass ratio 0.16 [18]. Howell acknowledged that due to the strong periodicity criterion required for computing halo orbits in case of the ER3BP, the number of halo orbits in the CR3BP that can be continued into the ER3BP is greatly reduced. Campagnola *et al*. also extended the Broucke method of finding periodic three-dimensional orbits in the ER3BP and stated Moulton's criterion of strong periodicity in a more general form [19]. The Broucke method of computing periodic orbits in the ER3BP has the drawback that many halo orbit solutions in the CR3BP cannot be continued into the ER3BP because they fail to satisfy Moulton's strong periodicity criterion [9]. Howell and Pernicka developed a different numerical method referred to as a "two-level" differential corrector to numerically compute Lissajous orbits in the CR3BP as well as in a higher fidelity ephemeris-based model [20], [21]. This method was presented in a

generalized form by Marchand *et al.* and was also extended to include various constraints on the solution [22]. In this work this method is used for computing periodic orbits in the ER3BP near SSSBs. It was found that using this method, any periodic solution from the CR3BP can be extended into the ER3BP. The resulting orbits were, however, found to be not exactly periodic as is detailed in Chapter 3. Hou and Liu computed a literal expansion for Lissajous and halo orbits in the ER3BP [23]. In the context of SSSBs, Szebehely computed the location of libration points in the CR3BP for bodies with mass ratios as small as 10^{-6} [2]. Scheeres and Marzari studied the motion of a spacecraft in the vicinity of a comet and found equilibrium solutions with solar gravitational and solar radiation pressure effects included [24]. They derived the equations of motion for a spacecraft in the vicinity of a comet in a coordinate frame centered at the comet and rotating with the comet about the Sun. He computed equilibrium solutions in this frame using second-order linearized equations with solar radiation pressure effects included. The level of the instability of the computed equilibrium points was analyzed using Floquet analysis [24]. A similar method is used in this work to determine the stability of the libration point orbits near SSSBs in the ER3BP.

Bennett has shown that all the collinear points in the ER3BP are unstable for any value of mass ratio and eccentricity [6]. The orbits in the vicinity of these unstable equilibrium points in the ER3BP are unstable except in a few cases [18]. As a result, station-keeping techniques are needed to maintain a spacecraft in these orbits. Farquhar designed a linear feedback controller for station-keeping to a second-order nominal solution using radial range and range rate feedback for x motion control [25]. He noted that even though the control accelerations were continuous, a pulsed control will behave

like a continuous one if the pulse frequency is much higher than any of the natural frequency of the system. Farquhar also designed an on-off control system design using limit cycle analysis. Breakwell *et al.* presented an optimal station-keeping controller that minimized the control cost and the position error margins [26]. It was assumed that the perturbations such as solar radiation pressure can be included in the nominal orbit and not in the feedback controller as they have insignificant effect on the controller performance. Howell and Pernicka proposed an optimal impulsive maneuver strategy that minimized a cost function that is a function of position error, velocity error and the applied maneuver magnitude [27]. This approach was also used for station-keeping of the Genesis mission [28]. A linear disturbance accommodating feedback controller was proposed by Cielaszyk and Wie, in which the spectral components of the nonlinear dynamics were subtracted from the control accelerations to minimize the station-keeping costs. The controller only requires the frequency of the nonlinear disturbances. The controller was applied to the station-keeping problem in the CR3BP model and used 140 m/s of ΔV per year for halo orbit station-keeping [29]. Gurfil and Meltzer extended the disturbance accommodating linear controller to the ER3BP [30]. Gomez *et al.* presented two different impulsive station-keeping approaches based on target points with cost minimization and Floquet mode cancellation for translunar libration point orbits [31]. A survey paper on station-keeping of libration point orbits in the Earth-Moon system was presented by Folta and Vaughn [32]. They implemented a differential correction targeting scheme and a discrete LQR controller and showed that with navigation errors, maneuver errors and SRP perturbation mismodeling, the ΔV costs for an Earth-Moon L_1 "small" halo orbit were close to 88 m/s/year for a *y*-axis control differential corrector and 61 m/s/year for

discrete LQR. Kulkarni *et al.* proposed an H_∞ approach for halo orbit station-keeping assuming continuous thrust. The H_∞ controller was applied to station-keep a spacecraft in a nominal orbit derived from a third-order solution with actual nonlinear dynamics taken from the CR3BP model. With inclusion of tracking error of 9 km and 4 mm/s in position and velocity and thruster limitations, the ΔV cost was close to 9 m/s for one halo orbit revolution [33]. Lincoln and Veres proposed a sliding mode controller for a 6-DOF control of a spacecraft in halo orbit with actual dynamics modeled as the CR3BP and using potential function guidance for position and attitude [34]. This was the only work found in the literature which used sliding mode approach for station-keeping of libration point orbits. In this work, a similar sliding mode controller is designed and applied in a higher fidelity ER3BP model with more realistic disturbance sources added in the simulation. Folta *et al.* provides a good summary of different station-keeping strategies and applies them to Lissajous orbits in the Earth-Moon system in the context of the ARTEMIS mission [35]. A long-term station-keeping strategy employing multiple-shooting differential corrector is proposed by Pavlak and Howell and applied to the ARTEMIS mission [36].

1.4. CONTRIBUTIONS

This work is primarily focused in two aspects of a small body mission design: to compute reference libration point trajectories in the vicinity of the small body and to design a robust station-keeping controller that can accommodate significant uncertainties

and still provide “tight” control. This thesis is organized into following sections as summarized below

Section 2

This section contains the background material that is the foundation of the methods detailed in the following sections. The differential equations of motion for the ER3BP (as well as the CR3BP) are derived. A brief description of the equilibrium points and the stability results for these solutions are given. The ER3BP differential equations in a libration-point centric frame are derived, which are later used in Setion 3. A typical differential corrector algorithm to compute halo orbits in the CR3BP is also given.

Section 3

The existence of the collinear libration points at a safe distance from the small body and the periodic orbits around these libration points are investigated. A two-level generalized multiple shooting differential corrector is described for continuation of halo orbits from the CR3BP into the ER3BP with significant eccentricity. The periodicity constraints necessary to compute a continuous orbit are also described.

Section 4

The stability analysis of the halo-like orbits computed in Section 3 using Floquet analysis is given.

Section 5

In this section, a robust three-axis sliding-mode control based station-keeping strategy is described for libration point orbits near small bodies. Various perturbation

effects are described and compensated for in the design of the SMC controller. The resulting trajectories along with the station-keeping costs are presented.

Section 6

The conclusions are presented and scope of future work is discussed.

2. BACKGROUND

2.1. THE ELLIPTIC RESTRICTED THREE-BODY PROBLEM

The Elliptic Restricted Three-Body Problem (ER3BP) defines a mathematical model to describe the motion of an infinitesimal particle under the influence of the gravity of two primary bodies. The infinitesimal particle, often considered a spacecraft, is assumed to not influence the motion of the primaries. Interestingly this simplified model has considerably more applications in space dynamics than the more general problem of describing the motion of a system of three gravitational bodies [2]. In the ER3BP, it is assumed that the smaller primary orbits around the larger primary in an elliptical orbit described by the two-body problem. A special case of the ER3BP is the Circular Restricted Three-Body Problem (CR3BP) in which the primaries move in circular orbits. The restricted three-body systems studied in this work define the Sun as the larger primary, a small solar system body such as an asteroid or a comet as the smaller primary and, a spacecraft as the infinitesimal mass.

This chapter provides the background that forms the basis of the material in the subsequent chapters. The equations of motion for the ER3BP as well as the CR3BP are derived. Lagrange has shown that the five equilibrium solutions called “Lagrange” or “libration” points exist in this system [2]. Three of these points exist on a straight line joining the two primaries and thus are called “collinear” points and the remaining two form two equilateral triangles with the two primaries. This study focuses on the spacecraft motion around the collinear points primarily near the L_1 and L_2 locations. An analytic series solution expanded to third-order for finding periodic orbits is used in this work is given by Richardson [15] that helps in finding initial conditions to initiate a

differential correction process used in the numerical algorithm. The last section describes this differential corrector used to find periodic halo orbits in the CR3BP.

2.2. EQUATIONS OF MOTION

This section shows the derivation of the ER3BP equations of motion (EOMs) including the CR3BP EOMs as a special case. The EOMs are first derived in terms of a coordinate frame with the origin fixed at the barycenter of two primary bodies. Later these equations are written relative to a coordinate frame translated to a collinear libration point (LP). The EOMs in the LP-centric frame are used in the two-level differential corrector algorithm to increase the numerical accuracy as shown in the following chapter.

2.2.1. The ER3BP. To derive the EOMs for the ER3BP, a synodic coordinate frame is defined with its origin attached to the barycenter of the two primaries and rotating with the smaller primary as shown in Figure 2.1. The larger primary in the figure is the Sun and the smaller primary shown is *25143 Itokawa* asteroid (note the figure is not to scale). Both bodies revolve around their barycenter "B" in an elliptic orbit. An inertial frame (X, Y, Z) is shown with its origin attached also at the barycenter. The locations of the three collinear points known as L_1, L_2 and L_3 are also shown. The **x** axis of the synodic frame always points towards the smaller primary, the **z** axis points in the direction of angular momentum vector associated with the motion of the two primaries and the **y** axis complete the right-handed triad. The mass of the larger and smaller primary is taken as m_1 and m_2 respectively.

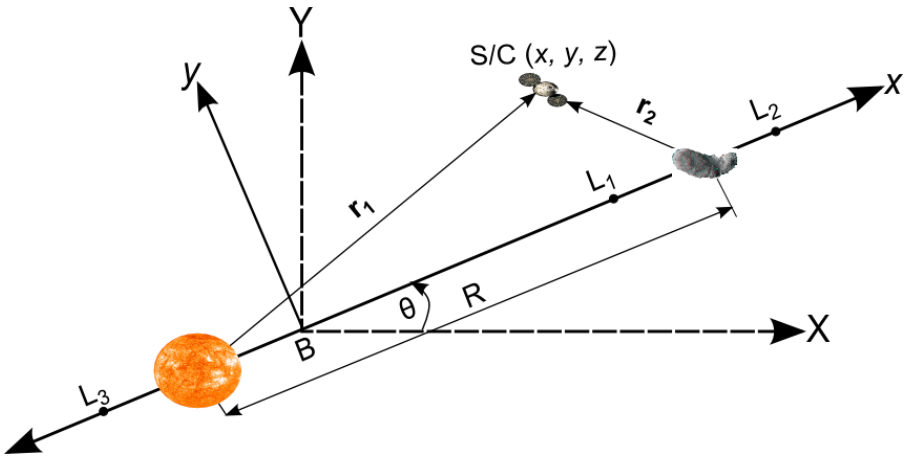

Figure 2.1. The Inertial and Synodic Coordinate Frames in the Sun-Small Body Restricted Three-Body Problem (Figure is not to scale).

Using Newton's second law and the law of gravitation, the EOMs are written as

$$\tilde{\mathbf{r}}'' = -\frac{Gm_1\mathbf{R}_1}{\|\mathbf{R}_1\|^3} - \frac{Gm_2\mathbf{R}_2}{\|\mathbf{R}_2\|^3} \tag{1}$$

where

$$\mathbf{R}_1 = \tilde{\mathbf{r}} - \mathbf{P}_1$$
$$\mathbf{R}_2 = \tilde{\mathbf{r}} - \mathbf{P}_2$$

In the above equation $\tilde{\mathbf{r}}, \mathbf{P}_1, \mathbf{P}_2$ represent the position vectors of the spacecraft,

larger primary and smaller primary respectively and *G* represents the gravitational constant. The $\tilde{x}$ and $\tilde{y}$ coordinates of the position vector $\tilde{\mathbf{r}}$ expressed in terms of the inertial frame can be conveniently transformed to the synodic frame using the following rotation expressed in terms of complex variables [2]

$$\begin{aligned} \tilde{\mathbf{r}} &= \bar{\mathbf{r}} e^{int}, n = \theta' \\ \tilde{\mathbf{r}}'' &= \left(\bar{\mathbf{r}}'' + i2\theta' \bar{\mathbf{r}}' + i\theta'' \bar{\mathbf{r}} - \theta'^2 \bar{\mathbf{r}} \right) e^{int} \end{aligned} \tag{2}$$

where

$$\begin{aligned} \tilde{\mathbf{r}} &= \tilde{x} + i\tilde{y} \\ \bar{\mathbf{r}} &= \bar{x} + i\bar{y} \end{aligned}$$

In the above equation $\bar{x}$ and $\bar{y}$ are the coordinates of the position vector of the spacecraft in terms of the synodic frame and *n* is the angular velocity of the smaller primary with respect to the inertial frame. Note that the *z* motion is not affected by this rotation. Note Eq. (1) expressed in terms of the synodic frame using the above rotation is

$$\left(\bar{\mathbf{r}}'' + i2\theta' \bar{\mathbf{r}}' + i\theta'' \bar{\mathbf{r}} - \theta'^2 \bar{\mathbf{r}} \right) e^{int} = -\frac{Gm_1 \bar{\mathbf{r}}_1 e^{int}}{\left\| \bar{\mathbf{r}}_1 \right\|^3} - \frac{Gm_2 \bar{\mathbf{r}}_2 e^{int}}{\left\| \bar{\mathbf{r}}_2 \right\|^3} \tag{3}$$

where

$$\bar{\mathbf{r}}_1 = \bar{\mathbf{r}} - \bar{\boldsymbol{\rho}}_1$$
$$\bar{\mathbf{r}}_2 = \bar{\mathbf{r}} - \bar{\boldsymbol{\rho}}_2$$

In the above equation $\bar{\mathbf{r}}$, $\bar{\boldsymbol{\rho}}_1$, $\bar{\boldsymbol{\rho}}_2$ are also the position vectors of the spacecraft, larger primary and smaller primary respectively and are expressed in terms of the synodic frame. Dimensionless coordinates are introduced in the above vector equation to show that the restricted problem only depends upon two parameters for the ER3BP. The following dimensionless coordinates for length, mass and time are introduced as

$$\mathbf{r} = \frac{\bar{\mathbf{r}}}{a}, \quad \boldsymbol{\rho}_1 = \frac{\bar{\boldsymbol{\rho}}_1}{a}, \quad \boldsymbol{\rho}_2 = \frac{\bar{\boldsymbol{\rho}}_2}{a} \tag{4}$$

$$\mu = \frac{m_2}{m_1 + m_2}, 1 - \mu = \frac{m_1}{m_1 + m_2} \tag{5}$$

$$\bar{t} = nt, \quad \frac{d}{d\bar{t}} = n\frac{d}{dt} \tag{6}$$

where t is the nondimensional time and a represents the semimajor axis of the orbit of the smaller primary around the larger primary and μ represents the mass ratio which is equal to the ratio of the mass of the smaller primary and the total mass of both primaries. Introducing the nondimensional variables from Eq. (4), (5), (6) into Eq. (3) gives

$$\ddot{\mathbf{r}} + 2i\dot{\theta}\dot{\mathbf{r}} + i\ddot{\theta}\mathbf{r} - \dot{\theta}^2\mathbf{r} = -\frac{G\left(m_1 + m_2\right)}{n^2 a^3}\left(\frac{\left(1-\mu\right)\mathbf{r}_1}{\left\|\mathbf{r}_1\right\|^3} + \frac{\mu\mathbf{r}_2}{\left\|\mathbf{r}_2\right\|^3}\right) \tag{7}$$

where

$$G\left(m_1 + m_2\right) = n^2 a^3$$
$$\mathbf{r}_1 = \mathbf{r} - \boldsymbol{\rho}_1$$
$$\mathbf{r}_2 = \mathbf{r} - \boldsymbol{\rho}_2$$

In the above equation $\boldsymbol{\rho}_1$, $\boldsymbol{\rho}_2$ are the position vectors of the larger and the smaller primary in terms of the nondimensional variables. Because the primaries lie on the *x* axis of the synodic frame, their *y* and *z* coordinates are identically zero. Their *x* coordinates in the synodic frame are calculated using the barycenter definition as

$$\begin{aligned} m_1\rho_{x1} - m_2\rho_{x2} &= 0 \\ \rho_{x1} + \rho_{x2} &= R \end{aligned} \tag{8}$$

which gives

$$\begin{aligned} \rho_{x1} &= \mu R \\ \rho_{x2} &= \left(1-\mu\right)R \end{aligned} \tag{9}$$

where *R* is the distance between the two primaries. Substituting the values of the location of the two primaries from Eq. (9) into the Eq. (7), the ER3BP equations in terms of the

nondimensional variables expressed in terms of the synodic frame coordinates can be written in scalar form as

$$\begin{aligned}
\ddot{x} - 2\dot{\theta}\dot{y} + \ddot{\theta}y - \dot{\theta}^2 x &= -\left(\frac{(1-\mu)(x+\mu R)}{\|\mathbf{r}_1\|^3} + \frac{\mu(x-1+\mu R)}{\|\mathbf{r}_2\|^3} \right) \\
\ddot{y} + 2\dot{\theta}\dot{x} + \ddot{\theta}x - \dot{\theta}^2 y &= -\left(\frac{(1-\mu)y}{\|\mathbf{r}_1\|^3} + \frac{\mu y}{\|\mathbf{r}_2\|^3} \right) \\
\ddot{z} &= -\left(\frac{(1-\mu)z}{\|\mathbf{r}_1\|^3} + \frac{\mu z}{\|\mathbf{r}_2\|^3} \right)
\end{aligned} \tag{10}$$

where

$$\begin{aligned}
r_1 &= \sqrt{(x+\mu R)^2 + y^2 + z^2} \\
r_2 &= \sqrt{(x-1+\mu R)^2 + y^2 + z^2}
\end{aligned}$$

It should be noted that the above equations for the ER3BP are not autonomous and depend explicitly on time through the angular velocity rate of the primary system $\dot{\theta}$.

2.2.2. The CR3BP. The CR3BP is a special case of the ER3BP model in which the primaries are assumed to move in circular orbits about the barycenter. As a result, the following simplifications can be made as

$$\dot{\theta} = 1,\ \ddot{\theta} = 0,\ R = 1 \tag{11}$$

Substituting these relations into Eq. (10), the CR3BP equations can be written as

$$\begin{aligned}\ddot{x}-2\dot{y}-x&=-\left(\frac{(1-\mu)(x+\mu)}{\|\mathbf{r}_1\|^3}+\frac{\mu(x-1+\mu)}{\|\mathbf{r}_2\|^3}\right)\\ \ddot{y}+2\dot{x}-y&=-\left(\frac{(1-\mu)y}{\|\mathbf{r}_1\|^3}+\frac{\mu y}{\|\mathbf{r}_2\|^3}\right)\\ \ddot{z}&=-\left(\frac{(1-\mu)z}{\|\mathbf{r}_1\|^3}+\frac{\mu z}{\|\mathbf{r}_2\|^3}\right)\end{aligned} \tag{12}$$

where

$$r_1=\sqrt{(x+\mu)^2+y^2+z^2}$$
$$r_2=\sqrt{(x-1+\mu)^2+y^2+z^2}$$

It should be noted that in contrast to the ER3BP, the CR3BP equations *are* autonomous and only depend upon the mass ratio μ.

An integral of motion exists for the CR3BP known as the Jacobian integral. To derive this invariant relation for the CR3BP a pseudo-potential function is first defined as [2]

$$\Omega=\frac{1}{2}\left(x^2+y^2\right)+\frac{1-\mu}{r_1}+\frac{\mu}{r_2} \tag{13}$$

Using the pseudo-potential the CR3BP EOMs can be succinctly written as

$$\begin{aligned} \ddot{x} - 2\dot{y} &= \frac{\partial \Omega}{\partial x} \\ \ddot{y} + 2\dot{x} &= \frac{\partial \Omega}{\partial y} \\ \ddot{z} &= \frac{\partial \Omega}{\partial z} \end{aligned} \tag{14}$$

Multiplying the three equations from Eq. (14) with $\dot{x}, \dot{y}, \dot{z}$ respectively and adding them together gives

$$\dot{x}\ddot{x} + \dot{y}\ddot{y} + \dot{z}\ddot{z} = \Omega_x \dot{x} + \Omega_x \dot{y} + \Omega_z \dot{z} \tag{15}$$

Integrating with respect to time gives the invariant relationship

$$\frac{1}{2}\left(\dot{x}^2 + \dot{y}^2 + \dot{z}^2\right) = \Omega + C \tag{16}$$

where the integration constant *C* is known as the Jacobi constant and the above relation is called the Jacobian integral. The Jacobian integral is the only known integral of motion for the CR3BP and can be used to define the accessible regions for a spacecraft with a given energy. It is known that for the ER3BP the Jacobian integral does not exist and the Jacobian constant *C* in the above relation changes with time and so do the regions accessible to a spacecraft with a given energy.

2.3. EQUILIBRIUM SOLUTIONS AND STABILITY CHARACTERISTICS

Five equilibrium are known to exist for the CR3BP EOMs as shown in Eq. (12). The libration points occur at the locations where the right hand sides of these equations vanish. In this section, the locations of the three collinear libration points, which lie on a line joining the two primaries, are computed. The same method is used to find the location of collinear libration points for a number of SSSB-like asteroids and comets in the following chapter.

The locations of the three collinear points L_1, L_2 and L_3 are shown in Figure 2.1. In the synodic frame the *y* and *z* coordinates are zero for all three collinear points and their respective *x* coordinates can be computed by equating the right-hand side of the *x* motion equation from Eq. (12) to zero as

$$\begin{aligned} \frac{\partial \Omega}{\partial x} &= 0 \\ x - \frac{(1-\mu)(x+\mu)}{r_1^3} - \frac{\mu(x-1+\mu)}{r_2^3} &= 0 \end{aligned} \tag{17}$$

The values of r_1 and r_2 in the above equation have a specific different value for each of the libration points based on their location, given as

$$\begin{aligned} L_1 &: r_1 = x+\mu,\ r_2 = 1-\mu-x \\ L_2 &: r_1 = x+\mu,\ r_2 = x-1+\mu \\ L_3 &: r_1 = -x-\mu,\ r_2 = 1-\mu-x \end{aligned} \tag{18}$$

The above relations are substituted in Eq. (14) to obtain three different quintic

polynomials for each of the collinear point as

$$\begin{aligned} &L_1 : \xi = 1-\mu-x \\ &\quad \xi^5 - (3-\mu)\xi^4 + (3-2\mu)\xi^3 - \mu\xi^2 + 2\mu\xi - \mu = 0 \\ &L_2 : \xi = 1-\mu+x \\ &\quad \xi^5 + (3-\mu)\xi^4 + (3-2\mu)\xi^3 - \mu\xi^2 - 2\mu\xi - \mu = 0 \\ &L_3 : \xi = 1-\mu-x \\ &\quad \xi^5 - (3-\mu)\xi^4 + (3-2\mu)\xi^3 - \mu\xi^2 + 2\mu\xi - \mu = 0 \end{aligned} \tag{19}$$

The quintic polynomials are numerically solved using the Newton-Raphson method to compute the location of the collinear points for a given value of the mass ratio. In the ER3BP, the libration point locations "oscillate" about their "mean" locations found in the CR3BP; however the ratio of the distance from the smaller primary to the libration point and the distance between the two primaries remains constant in the CR3BP as well as in the ER3BP. This constant γ has a specific value for each libration point and is given as

$$\gamma_{L_i} = \frac{\xi}{R} \tag{20}$$

Szebehely [2] gives an analytic series solution for the above constants as shown below in Eq. (21). The same series through order 11 is given by Richardson and Cary [14].

$$\begin{aligned} \gamma_{L_1} &= \nu\left(1 - \frac{1}{3}\nu - \frac{1}{9}\nu^2 - \frac{23}{81}\nu^3 + \frac{151}{243}\nu^4 - \frac{1}{9}\nu^5\right) + o\left(\nu^7\right) \\ \gamma_{L_2} &= \nu\left(1 + \frac{1}{3}\nu - \frac{1}{9}\nu^2 - \frac{31}{81}\nu^3 - \frac{119}{243}\nu^4 - \frac{1}{9}\nu^5\right) + o\left(\nu^7\right) \end{aligned} \tag{21}$$

where

$$\nu = \left(\frac{\mu}{3(1-\mu)} \right)^{\frac{1}{3}}$$

It should be noted that in the CR3BP $\gamma = \xi$ as the distance between the primaries is unity in nondimensional units. Once the values of γ for each collinear libration point are found in the CR3BP, their instantaneous locations in the ER3BP at a given time are computed using Eq. (20).

All three collinear libration points are known to be unstable in the CR3BP as well as the ER3BP. In the CR3BP, the stability can be analyzed by linearizing the EOMs about the libration point and computing the eigenvalues of the linearized dynamics matrix. The linearized EOMs are given in the following section. In the linearized system, the out-of-plane motion decouples from the in-plane motion. For the in-plane motion two out of the four eigenvalues are positive and thus the in-plane motion is unstable for any value of the mass ratio. However, for the triangular equilibrium points a range of mass ratio exists for which the eigenvalues are purely imaginary and thus marginally stable. Similar to the CR3BP, in the ER3BP all three collinear points are unstable for any value of the mass ratio and the eccentricity [6].

2.4. PERIODIC SOLUTIONS NEAR LIBRATION POINTS

This section first details the ER3BP equations of motion in a libration point-centric (LP-centric) coordinate frame. These equations of motion are used in the two-step differential correction algorithm described in Chapter 3 for numerically computing quasi-periodic three-dimensional orbits in the ER3BP. The linearlized EOMs are given in the following subsection which can be used to show that the three-dimensional infinitesimal periodic orbits can exist near the collinear libration points if appropriate initial conditions are chosen.

2.4.1. The ER3BP EOMs in the Libration Point Frame. Expressing the ER3BP EOMS in a LP-centric frame can be accomplished by introducing a translation to the barycentric EOMs given by Eq. (10) as

$$\begin{aligned} x_{TB} &= x_{TL} + x_{LB} \\ x_{LB} &= \left(1 - \mu \mp \gamma_L\right) R \end{aligned} \tag{22}$$

where x_{TB} and x_{TL} are the abscissa coordinates of the third body or spacecraft in the barycentric and the LP-centric coordinate frames respectively. The upper sign in Eq. (22) applies to the L_1 and the lower applies to the L_2 libration point.

2.4.2. Linearized Dynamics. The EOMs linearized about a libration point can be used to find particular solutions that may exist in the regions near the libration points. It can also be shown that particular periodic solutions exist in the vicinity of the libration points in the CR3BP as well as in the ER3BP. In general the frequency of the linearized in-plane and out-of-plane motions are not equal. This results in orbits that appear

as Lissajous figures when observed from certain viewpoints and are referred to as "Lissajous" orbits. However, if the amplitude of the in-plane motion is sufficiently large, then the nonlinear contributions can be used to make the two frequencies equal. The resulting trajectories are three-dimensional periodic orbits and are called "halo" orbits, a term first coined by Farquhar [11] . The following section describes a differential correction process that can be used to find initial conditions for halo orbits in the CR3BP. The linearized equations are used to compute the state transition matrix (STM) that is used in the differential correction algorithm. In Chapter 3, a method to find halo-like orbits in the ER3BP is presented. The ER3BP EOMs given by Eq. (10) can be linearized about a collinear libration point whose location x_{LB} is given by Eq. (22). The resulting linearized dynamics can be written in the matrix form as

$$\begin{bmatrix} \delta\dot{x} \\ \delta\dot{y} \\ \delta\dot{z} \\ \delta\ddot{x} \\ \delta\ddot{y} \\ \delta\ddot{z} \end{bmatrix} = \begin{bmatrix} 0 & 0 & 0 & 1 & 0 & 0 \\ 0 & 0 & 0 & 0 & 1 & 0 \\ 0 & 0 & 0 & 0 & 0 & 1 \\ \Omega_{xx} & \Omega_{xy}+\ddot{\theta} & \Omega_{xz} & 0 & 2\dot{\theta} & 0 \\ \Omega_{xy}-\ddot{\theta} & \Omega_{yy} & \Omega_{yz} & -2\dot{\theta} & 0 & 0 \\ \Omega_{xz} & \Omega_{yz} & \Omega_{zz} & 0 & 0 & 0 \end{bmatrix} \begin{bmatrix} \delta x \\ \delta y \\ \delta z \\ \delta\dot{x} \\ \delta\dot{y} \\ \delta\dot{z} \end{bmatrix} \tag{23}$$

where $\delta x, \delta y, \delta z$ are the deviations from a libration point and the subscripts represents derivative with respect to that variable. The symbol Ω is the pseudo-potential function for the ER3BP in the LP centric frame and is given as

$$\Omega = \frac{1}{2}\dot{\theta}^2\left(x^2+y^2\right)+\frac{1-\mu}{r_1}+\frac{\mu}{r_2} \tag{24}$$

where

$$r_1 = \sqrt{\left(x + (1 \mp \gamma_L)R\right)^2 + y^2 + z^2}$$
$$r_2 = \sqrt{\left(x \mp \gamma_L R\right)^2 + y^2 + z^2}$$

The *x*, *y* and *z* are the third body coordinates in a LP-centric frame. The upper sign applies to L_1 and the lower sign applies to L_2.

2.4.3. Linearized Periodic Solutions. Periodic solutions are known to exist around collinear as well as triangular libration points. Although, the collinear libration points are unstable, conditional stability can exist when selecting initial conditions that suppress the unstable modes. For appropriately selected initial conditions, linearized solutions around collinear libration points can be shown to exist as

$$\begin{aligned} \delta x &= A_x \cos(\beta t + \phi) \\ \delta y &= -K_2 A_x \sin(\beta t + \phi) \\ \delta z &= A_z \cos(\sqrt{A}t + \psi) \end{aligned} \tag{25}$$

where

$$K_2 = \frac{1}{2\beta}\left(\beta^2 + 2A + 1\right)$$
$$A = \frac{1-\mu}{\left|x_L + \mu\right|^3} + \frac{\mu}{\left|x_L + 1 - \mu\right|^3}$$

The symbol x_L represents the particular collinear libration point abscissa coordinate. The parameters A_x, A_z, ϕ and ψ are chosen based on the desired periodic orbit around the collinear libration point. The value of β is the magnitude of the imaginary root of the polynomial

$$\lambda^4 + (2 - A)\lambda^2 + (1 + A - 2A^2) = 0 \tag{26}$$

A periodic solution can be found using Eq. (25) if the in-plane frequency β and out-of-plane frequency $\sqrt{A}$ can be made equal. Generally these two frequencies are not equal; however it can be shown that if the in-plane amplitude is sufficiently large, the nonlinear contributions can be used to make the two frequencies equal and perfectly periodic three-dimensional halo orbits can be found. The minimum amplitude required to make the two frequencies equal can be found by expanding the CR3BP equations up to third-order and using the Lindsedt-Poincaré method as shown by Richardson [15].

The stability of the periodic orbits about collinear libration points can be analyzed using the monodromy matrix. The monodromy matrix is computed by integrating the state transition matrix (STM) for exactly one complete time period. To demonstrate stability the modulus of the eigenvalues of the monodromy matrix must be equal to one. It can be shown that for a halo orbit in the CR3BP, the eigenvalues of the monodromy matrix occur in reciprocal pairs. Two of the six eigenvalues are real and found to be unity. The remaining four eigenvalues are complex and can be used to assess and compare the stability of the periodic orbits. In Section 4, the eigenvalues of the

monodromy matrix associated with periodic orbits computed near the SSSB in the ER3BP are computed and analyzed for stability.

2.5. NUMERICAL COMPUTATION OF HALO ORBITS IN THE CR3BP

The halo orbits can be found in the CR3BP by employing a differential correction algorithm that successively corrects the initial conditions to find periodic orbits. This is an iterative method that requires a sufficiently accurate initial condition to start the correction process. The initial conditions must be close enough to the actual solution in order for the algorithm to converge. To find/estimate the first "guess" of the initial conditions, a third-order analytic solution given by Richardson [15] for the halo orbits in the CR3BP is used in this work. The initial conditions from this analytic solution were found to be sufficiently accurate to ensure convergence for a wide-range of mass ratios from that of the Sun-Earth system to that of the Sun-*1999 AO10* asteroid system as shown in the following chapter.

In this section, a differential correction algorithm is summarized as originally given by Howell [17] to compute the halo orbits in the CR3BP. This differential correction algorithm takes advantage of the symmetry property of halo orbits. It can be seen that the CR3BP EOMs are invariant under the transformation

$$(t; x, y, z) \leftrightarrow (-t; x, -y, z) \tag{27}$$

The above invariant transformation indicates that periodic three-dimensional halo orbits may exist if they are symmetric with respect to the *x*-*z* plane. Additionally, for a periodic smooth solution, the orbit must cross the *x*-*z* plane orthogonally. As a result, if an initial condition in this plane is chosen, it must be in the vector form

$$\mathbf{x}_0 = \left[x_0, 0, z_0, 0, \dot{y}_0, 0\right]^T \tag{28}$$

where the superscript *T* denotes the transpose. As mentioned in this work, the initial conditions originating in the *x*-*z* plane are chosen from the analytic third-order solution. To find a periodic orbit, another perpendicular crossing at the half time period is required. If at the crossing of the *x*-*z* plane, the *x* and *z* velocities are not both zero then the non-zero magnitudes of these velocities can be used to correct the initial conditions to find an orthogonal crossing. The differential correction algorithm is started by integrating the six CR3BP EOMs along with the thirty-six scalar equations of the six-dimensional STM matrix. The integration is propagated until the trajectory crosses the *x*-*z* plane; let the time at that instant be T/2. The dependence of the state at time T/2 on the initial conditions can be linearly estimated using the STM as

$$\delta\mathbf{x}_{T/2} = \phi(T/2, 0)\delta\mathbf{x}_0 + \left.\frac{\partial\mathbf{x}}{\partial t}\right|_{t=T/2} \delta(T/2) \tag{29}$$

where ϕ is the STM. The above vector equation represents six scalar equations. The value of $\delta(T/2)$ can be expressed in terms of the initial conditions using the

second scalar equation of the above equation and noting that $\delta y = 0$ as

$$\delta y = 0 = \phi_{21}\delta x_0 + \phi_{23}\delta z_0 + \phi_{25}\delta \dot{y}_0 + \dot{y}_{T/2}\delta(T/2) \tag{30}$$

The three control variables $(x_0, z_0, \dot{y}_0)$ can be modified in order to force the two target variables $(\dot{x}_{T/2}, \dot{z}_{T/2})$ to be reduced to zero. As a result, there is the option of modifying only two of the three control variables. If x_0 is kept fixed, then the change in the initial conditions required to enforce a perpendicular crossing at T/2 can be written using Eq. (29) and Eq. (30) as

$$\begin{bmatrix} \delta \dot{x} \\ \delta \dot{z} \end{bmatrix} = \begin{bmatrix} -\dot{x}_{T/2} \\ -\dot{z}_{T/2} \end{bmatrix} = \left[\begin{bmatrix} \phi_{43} & \phi_{45} \\ \phi_{63} & \phi_{45} \end{bmatrix} - \frac{1}{\dot{y}_{T/2}} \begin{bmatrix} \ddot{x}_{T/2} \\ \ddot{z}_{T/2} \end{bmatrix} \begin{bmatrix} \phi_{23} & \phi_{23} \end{bmatrix} \right] \begin{bmatrix} \delta z_0 \\ \delta \dot{y}_0 \end{bmatrix} \tag{31}$$

Alternatively if z_0 is kept fixed instead, then the correction equation can be written as

$$\begin{bmatrix} \delta \dot{x} \\ \delta \dot{z} \end{bmatrix} = \begin{bmatrix} -\dot{x}_{T/2} \\ -\dot{z}_{T/2} \end{bmatrix} = \left[\begin{bmatrix} \phi_{41} & \phi_{45} \\ \phi_{61} & \phi_{45} \end{bmatrix} - \frac{1}{\dot{y}_{T/2}} \begin{bmatrix} \ddot{x}_{T/2} \\ \ddot{z}_{T/2} \end{bmatrix} \begin{bmatrix} \phi_{21} & \phi_{25} \end{bmatrix} \right] \begin{bmatrix} \delta x_0 \\ \delta \dot{y}_0 \end{bmatrix} \tag{32}$$

The above correction equations are applied in an iterative manner to successively reduce the value of target variables to zero.

3. PERIODIC ORBITS NEAR SMALL BODIES

3.1. SMALL SOLAR SYSTEM BODIES

The focus in space exploration has recently shifted to small solar system bodies such as asteroids and comets. The rationale behind this focus is due to the scientific knowledge that can be gained from their returned samples and also the threat posed by some of these bodies as they come close to Earth in their heliocentric orbits. A key challenge before NASA is the prospect of sending a human mission to an asteroid. A number of recent missions such as Dawn have been sent to small bodies and others are planned in the future. One of these robotic missions, Hayabusa, has even returned samples from the near-Earth *25143 Itokawa* asteroid. In contrast to the robotic missions, a human mission to a small body will involve many more challenges. For most small bodies the observation of mass, rotational periods, rotational axis, etc. are not available with desired accuracy. This necessitates the use of robust methods that can accommodate uncertain environments in a failsafe manner.

In this work a design for small body missions is considered that uses libration point orbits of the Sun-Small Body system. Similar to the missions to libration point orbits of the Sun-Earth or Earth-Moon systems, missions to small body libration point orbits (LPO) will also enjoy benefits including fewer/no communication blackouts, low ΔV costs for stationkeeping, and good overall mission flexibility. In addition these orbits will also provide a safe parking orbit for a “mothership” from which a small probe or a lander carrying humans can descend to the surface of the small body. These parking orbits will also be safe from uncertain environmental conditions close to the surface such as outgassing jets. With this mission design in view, a number of small body objects in

this work are considered based on their size, distance from Earth and feasibility for future missions. A list containing small body names and known physical properties was compiled from various NASA websites and is shown in Table 3.1. The list contains a number of small bodies ranging in size 0.1 km to 900 km in diameter. The list also includes the asteroid *1999 AO10* which is a potential candidate for a human mission to an asteroid. Because an estimate of the mass of *1999 AO10* could not be found, its mass was approximated by scaling the mass of the asteroid *1566 Icarus*. The following section describes an analysis of the existence of libration points and the size of halo orbits for these small bodies. It should be noted that the methods used in this work are completely general and apply to bodies of any size.

Table 3.1. List of Small Solar System Bodies[2].

Small Body	Mass x10^{15} [kg]	Size [km]	SMA [AU]	Ecc.	L_1 Distance [km]	L_2 Distance [km]	Minimum A_x (L_1) [km]	Minimum A_x (L_2) [km]
1999 AO10	0.00000036	0.1	0.911	0.1109	5.34887	5.34887	0.736304	0.736304
1566 Icarus	0.001	1.4	1.078	0.8269	88.9102	88.9102	12.2390	12.2390
433 Eros	6.69	33x13x13	1.458	0.2229	2,265.85	2,265.86	311.902	311.916
253 Mathilde	103.3	66x48x46	2.646	0.2660	10,239.7	10,239.8	1,409.49	1,409.64
140 Siwa	150	103	2.734	0.2157	11,980.9	11,981.2	1,649.17	1,649.36
45 Eugenia	6,100	226	2.721	0.0831	41,003.7	41,006.5	5,643.44	5,645.77
3 Juno	20,000	240	2.669	0.2579	59,749.8	59,755.7	8,222.81	8,227.85
4 Vesta	300,000	530	2.362	0.0895	130,397	130,429	17,938.5	17,965.7
1 Ceres	870,000	960x932	2.767	0.0789	217,824	217,900	29,957.7	30,022.4

[2] Physical and orbital parameters are taken from the JPL Small-Body Database http://ssd.jpl.nasa.gov/ and the webpage http://nssdc.gsfc.nasa.gov/planetary/factsheet/asteroidfact.html.

3.2. FEASIBILITY OF HALO-LIKE ORBITS NEAR SMALL BODIES

All the small bodies shown in Table 3.1 have an extremely small mass ratio in the Sun-Small Body system. For comparison the mass ratio for the Sun-Earth system is of the order of $3x10^{-6}$ while the *largest* small body from Table 3.1 the dwarf planet *1 Ceres,* has the mass ratio of the order of $3x10^{-15}$ in the Sun-*1 Ceres* system. Szebehely [2] has shown that the collinear libration points and the periodic orbits about them exist for all values of the mass ratio. However the libration points also need to be at a sufficient distance from the surface of the small body so that the third body in an orbit around the libration point does not collide with its surface. Additionally the extremely small mass ratio in the case of small bodies can result in significant errors in the precision of the numerical integration. The next subsection describes the computation of the location of collinear libration points L_1 and L_2 for a range of small mass ratios. Next, the minimum size of feasible halo orbits is computed using a 3^{rd}-order analytic solution in the CR3BP originally given by Richardson [15].

3.2.1. Libration Point Locations. To demonstrate that the halo-like orbits are feasible near small bodies, the CR3BP model was first used to compute the distance of the collinear libration point locations from the smaller primary in the Sun-small body system. The locations of L_1 and L_2 in the synodic frame were calculated by solving the quintic polynomials as shown in the previous chapter for a range of values of mass ratios. To show the variation of the distance of the libration points from the small body with respect to the mass ratio, the semimajor axis of the small body's orbit was arbitrarily set to 1 AU. Szebehely [2] showed that the distance between the smaller primary and collinear libration points $L_{1/2}$ increases monotonically with the mass ratio. This is evident

from the plot for the L_1 distance (from the small body) versus mass ratio as shown in Figure 3.1. It should be noted that the slope of the plot is steeper for small values of mass ratios compared to the larger ones, which is beneficial in establishing the existence of a

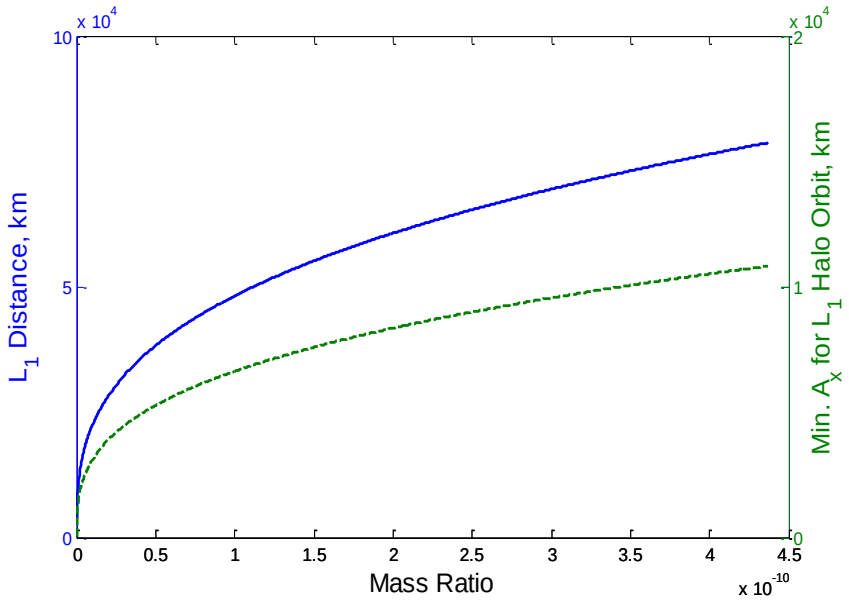

Figure 3.1. Variation of L_1 Distance from the Smaller Primary and the Minimum A_x Amplitude of Halo orbits.

libration point at a safe distance from the small body surface. Very similar results to those shown in Figure 3.1 are also found for the L_2 libration point. Table 3.1 lists the location of L_1 and L_2 libration points calculated for some small bodies using their true semimajor axes. The smallest body considered was *1999 AO10* for which the L_1 point exists at a safe distance of approximately 5.349 km from its center.

1999 AO10 is a Near-Earth Object (NEO) and is a possible destination for a human mission and its diameter is less than 0.1 km. Because in the elliptic problem the libration points oscillate about the "mean" positions found using the CR3BP model, these data only give an indication that the libration points exist at a safe distance from the smaller primary and can potentially host a viable halo and/or Lissajous orbit. The maximum "amplitude" of the libration point oscillation in the ER3BP can be found by computing the value of the constant γ_L numerically using Eq. (20) or analytically using Eq. (21). For *1999 AO10,* the γ_L value for both L_1 and L_2 are approximately the same and is 39.22×10^{-9}. Using the semi-major axis and the eccentricity of *1999 AO10* from Table 3.1, the minimum and maximum distances for the both libration points to *1999 AO10* are 4.755 km and 5.942 km respectively. Similarly for the dwarf planet *1 Ceres*, L_1 and L_2 exist at a distance of 217.8×10^3 km and 217.9×10^3 km, respectively from the body in the CR3BP. For L_1, the minimum and maximum distances from *1 Ceres* are 200.6×10^3 km and 235.0×10^3 km respectively with similar values were observed for L_2.

3.2.2. Minimum Halo Orbit Amplitude. Having established the existence of collinear libration points at a safe distance from the small body in the Sun-small body system, the minimum size of feasible halo orbits is computed next using the third-order analytic approximation for the halo orbits in the CR3BP. It is well known that halo orbits in the CR3BP only exist above some minimum in-plane amplitude that is dependent on the mass ratio. In particular, with the proper amplitude combination specified, the nonlinear contributions of the CR3BP equations of motion drive the eigen-frequencies of the in-plane motion to equal that of the out-of-plane motion, creating a halo orbit that repeats with each revolution about the libration point. Richardson's analytic solution [15]

showed that to match these eigen-frequencies the in-plane and out of plane amplitudes must satisfy

$$l_1 A_x^2 + l_2 A_z^2 + \Delta = 0 \tag{33}$$

where Δ is the frequency correction needed to match the in-plane and out-of-plane eigen-frequencies and l_1 and l_2 are constants. The details for calculating these parameters are given in Reference [15]. The minimum *x* amplitude A_x is found by setting the *z* amplitude A_z to zero in the above relationship. Figure 3.1 shows the plot of the halo orbit in-plane minimum A_x amplitude versus a range of mass ratios of the Sun-small body system in the CR3BP. Again the semi-major axis for each case is taken as 1 AU to show the variation of minimum halo size with the mass ratio. Because A_z is often a more useful parameter to specify during mission design, the minimum A_x value is used to select a value for the A_z amplitude for the desired halo orbit. Once the desired value of the A_z amplitude was chosen based on the desired size of the halo orbit, the corresponding *y*-component of velocity given by the analytic solution is fixed. Because the analytic solution is only developed through third-order, differential corrections are required to modify these initial conditions to produce a periodic halo orbit in the nonlinear CR3BP model as described in the previous chapter. The halo orbit symmetry with respect to the *x*-*z* plane is used to correct the initial *x*-component position and the magnitude of the *y* velocity iteratively to obtain a periodic halo orbit. Using this method, an L_2 halo orbit in the CR3BP for the Sun-*1999 AO10* system was calculated as shown in Figure 3.2. Suitable initial conditions for integrating a halo orbit for all the bodies in Table 3.1 were successfully found,

however numerical integrations for smaller bodies such as *1999 AO10* required significant more computational time than in the case of larger bodies due to the very small acceleration values in the former case. The *MATLAB* ode113 integrator is used to propagate all the reference orbits in this section with the relative tolerance taken as 10^{-13} and absolute tolerance as 10^{-16} for all the state elements.

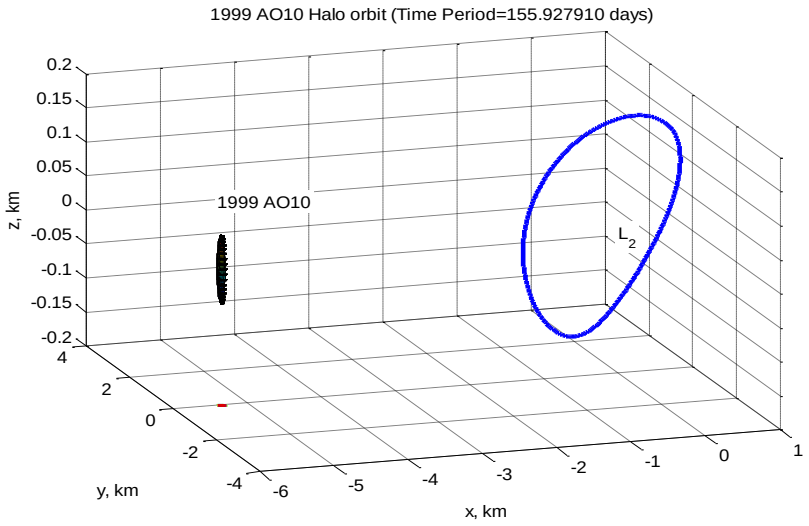

Figure 3.2. An L_2 Halo Orbit in the Sun-*1999 AO10* System (*1999 AO10* Drawn to Scale).

3.3. PERIODIC ORBITS IN THE ER3BP

Most small solar system bodies, including Near Earth Objects (NEOs), move in orbits with significant values of eccentricity that are typically much more than that of Earth's orbit, as seen in Table 3.1. The EOMs for the ER3BP depend explicitly on the angular rate of the primaries' orbit and thus on their corresponding eccentric anomaly. The Jacobi integral no longer exists as a result. Broucke showed that periodic Lyapunov

orbits can be numerically computed in the ER3BP for all values of eccentricity ranging from 0 to 1 [9]. He used Moulton's criteria of strong periodicity to find eligible periodic orbits in the CR3BP that can be numerically continued in the ER3BP. Campagnola *et al.* extended this method to compute three-dimensional halo orbits and successfully computed halo orbits in the Sun-Mercury and Earth-Moon systems [19]. The strong periodicity criterion states that the periodic orbits in the ER3BP must cross the *x*-*z* plane when the primaries are at an apse. In order to find such orbits, a periodic orbit was first found in the CR3BP with *M* revolutions during which time the primaries complete exactly *N* revolutions. These orbits then can be numerically continued in the ER3BP using differential corrections as given by Broucke [9]. Although this method furnishes perfectly periodic orbits in the ER3BP, the periodicity criterion severely restricts the number of orbits in the CR3BP that can be successfully continued in the ER3BP. Campagnola *et al.* found a three-dimensional periodic orbit in the Earth-Moon system that is in 2:1 resonance with the primary motion [19]. This orbit has a very large A_z amplitude compared to typical halo orbits in the Earth-Moon system and is significantly displaced toward the Moon from the L_2 point. In this work, a different numerical method is used to find halo-like periodic orbits in the ER3BP with significant eccentricity that can be used to continue any halo orbit from the CR3BP model into the ER3BP. This method, referred to as the "two-level differential corrector", was first proposed by Howell and Pernicka [20],[21] for numerically computing Lissajous orbits in the ER3BP as well as in an ephemeris-based model. Marchand *et al.* generalized this method and introduced periodicity constraints for finding periodic orbits [22].

The most precise measurements show that planetary as well as small bodies do not move in perfect elliptical orbits due to various perturbation forces acting on them. As a result for a NEO mission design using libration point orbits; it is imperative that existence of these orbits be analyzed in a higher fidelity ephemeris-based model. In this work the generalized two-level differential corrector method is used in finding halo-like orbits in the ER3BP. In contrast to the earlier work described, the trajectories are integrated using the LP-centric coordinates in place of the barycentric coordinates. It was found that the accuracy of the integration increased as well as the rate of convergence of the differential corrections by a factor of at least ten in many cases. This is due to the fact that in the barycentric frame the magnitude of the *x* coordinate of the libration point orbit is much greater than the corresponding *x* coordinate in the LP-centric frame. This decreases the numerical integration accuracy with fixed relative error control of the *x* coordinate. In addition, performing integration and differential corrections in the same LP-centric frame avoids the need of transforming target points repeatedly between the two frames during numerical continuation with increasing eccentricity. (It should be noted that the conversion between the barycentric and LP-centric frame also require numerically solving Kepler's equation.)

3.3.1. Two-Level Differential Corrector. The Level-1/Level-2 differential correction algorithm is reproduced here from References [20], [22]. The entire process is typically repeated four to five times to obtain a completely continuous orbit, within numerical tolerance. The halo orbits near small bodies computed in the CR3BP as shown in Subsection 2 are used to start the numerical continuation process with nonzero primary eccentricity now introduced. The CR3BP halo orbit is divided into a number of

segments. The starting point of each segment is chosen as a target point with position and velocity states defined from the initial estimate. The Level-1 algorithm computes corrections to the three velocity states of the initial point of each segment in order to drive the error between the final state on the current segment and the initial position states of the next segments to negligibly small values. The time of flight can also be corrected to meet the desired tolerance level. To derive the generalized correction equation, consider a contemporaneous variation in the state using

$$\delta\mathbf{x}(t_1) = \phi(t_1, t_0)\,\delta\mathbf{x}(t_0) \tag{34}$$

where ϕ is the STM and $\delta\mathbf{x}(t)$ is the variation in the value of $x(t)$ at time t_1 due to the variation at the time t_0. A noncontemporaneous variation can be written as

$$\delta\mathbf{x}(t') = \delta\mathbf{x}(t) + \dot{\mathbf{x}}(t)\delta t \tag{35}$$

Using Eq. (34) and (35), the generalized differential correction equation can be written as

$$\left[\delta\mathbf{x}(t_1') - \dot{\mathbf{x}}(t_1)\delta t_1\right] = \phi(t_1, t_0)\left[\delta\mathbf{x}(t_0') - \dot{\mathbf{x}}(t_0)\delta t_0\right] \tag{36}$$

If the initial time is not varied in the correction process i.e. δt_0 =0, the above equation can be simplified to

$$\delta \mathbf{x}(t_1') = \phi(t_1, t_0)\delta \mathbf{x}(t_0') + \dot{\mathbf{x}}(t_1)\delta t_1 \tag{37}$$

In Level-1 corrections, the above equation is used to reduce the position discontinuities between the segments. Consider two trajectory segments 1 and 2 derived from a starting solution with the corresponding target points $(t_1, \mathbf{x}_1)$ and $(t_2, \mathbf{x}_2)$ respectively. After a parameter such as eccentricity is perturbed, the new first segment is integrated along with the state transition matrix using the first target point until time t_2. The new state $(t_2, \mathbf{x}_2')$ at time t_2 can be represented in terms of the first target point using Eq. (37) as

$$\delta \mathbf{x}_2' = \phi(t_2, t_1)\delta \mathbf{x}_1 + \left.\frac{\partial \mathbf{x}'}{\partial t}\right|_{t_2} \delta(t_2 - t_1) \tag{38}$$

In the above differential correction equation, there are four "free" variables $\delta \dot{x}_1, \delta \dot{y}_1, \delta \dot{z}_1, \delta(t_2 - t_1)$ and three target variables $\delta x_2', \delta y_2', \delta z_2'$. A linear least square error solution can be found for Eq. (31) by arranging it in an over-determined system of linear equations as

$$A\mathbf{x} = B \tag{39}$$

where

$$A = \begin{bmatrix} \phi_{14} & \phi_{15} & \phi_{16} & \dot{x} \\ \phi_{24} & \phi_{25} & \phi_{26} & \dot{y} \\ \phi_{34} & \phi_{35} & \phi_{36} & \dot{z} \end{bmatrix}_{t_2}$$

$$\mathbf{x} = \begin{bmatrix} \delta\dot{x}_1 \\ \delta\dot{y}_1 \\ \delta\dot{z}_1 \\ \delta(t_2 - t_1) \end{bmatrix}, \quad B = \begin{bmatrix} \delta x_2' \\ \delta y_2' \\ \delta z_2' \end{bmatrix} = \begin{bmatrix} x_2 - x_2' \\ y_2 - y_2' \\ z_2 - z_2' \end{bmatrix} \tag{40}$$

A minimum error solution of the above under-determined system of equations can be given as

$$\mathbf{x} = A^T (AA^T)^{-1} B \tag{41}$$

After the first iteration, the corrections **x** are applied to the first target point and the above process is repeated until all the elements of the *B* vector in the above equations reduce to values below the tolerance level. The same process is repeated for each of the segment of the trajectory. At the end of this complete process, an orbit composed of a number of segments is obtained that is continuous in position and discontinuous in velocity at each target point. The velocity discontinuities are subsequently reduced in the Level-2 correction.

In the Level-2 differential correction, the velocity discontinuities at all the target points except the first and the last one are reduced in a single step by adjusting the position and time of each of the target points. To derive the Level-2 correction equation, the generalized differential corrector is used [22]. For Segment 1, the variational equation can be written using Eq. (36) as

$$\begin{bmatrix} \delta\mathbf{r}_2'^{-} - \mathbf{v}_2^{-}\delta t_2^{-} \\ \delta\mathbf{v}_2'^{-} - \mathbf{a}_2^{-}\delta t_2^{-} \end{bmatrix} = \begin{bmatrix} A_{21} & B_{21} \\ C_{21} & D_{21} \end{bmatrix} \begin{bmatrix} \delta\mathbf{r}_1'^{+} - \mathbf{v}_1^{+}\delta t_1^{+} \\ \delta\mathbf{v}_1'^{+} - \mathbf{a}_1^{+}\delta t_1^{+} \end{bmatrix} \tag{42}$$

Solving the first equation of the above matrix equation for $\delta\mathbf{v}_1'^{+}$ and substituting its expression in the second equation, the following expression for the velocity at Target Point 2 on Segment 1 is found as

$$\begin{aligned} \delta\mathbf{v}_2'^{-} = &\left(C_{21} - A_{21}B_{21}^{-1}D_{21}\right)\delta\mathbf{r}_1'^{+} - \left(C_{21} - A_{21}B_{21}^{-1}D_{21}\right)\mathbf{v}_1^{+}\delta t_1^{+} \\ &+ D_{21}B_{21}^{-1}\delta\mathbf{r}_2'^{-} + \left(\mathbf{a}_2^{-} - D_{21}B_{21}^{-1}\mathbf{v}_2^{-}\right)\delta(t_2^{-}) \end{aligned} \tag{43}$$

Similarly the variational equation for Segment 2 with integration direction backwards from Target Point 3 to Target Point 2 can be written as

$$\begin{bmatrix} \delta\mathbf{r}_2'^{+} - \mathbf{v}_2^{+}\delta t_2^{+} \\ \delta\mathbf{v}_2'^{+} - \mathbf{a}_2^{+}\delta t_2^{+} \end{bmatrix} = \begin{bmatrix} A_{23} & B_{23} \\ C_{23} & D_{23} \end{bmatrix} \begin{bmatrix} \delta\mathbf{r}_3'^{-} - \mathbf{v}_3^{-}\delta t_3^{-} \\ \delta\mathbf{v}_3'^{-} - \mathbf{a}_3^{-}\delta t_3^{-} \end{bmatrix} \tag{44}$$

Using the above equation the expression for the velocity at Target Point 2 on Segment 2 as

$$\begin{aligned} \delta\mathbf{v}_2^{+} = &D_{23}B_{23}^{-1}\delta\mathbf{r}_2'^{+} + \left(\mathbf{a}_2^{+} - D_{23}B_{23}^{-1}\mathbf{v}_2^{+}\right)\delta t_2^{+} + \left(C_{23} - D_{23}B_{23}^{-1}A_{23}\right)\delta\mathbf{r}_3'^{-} \\ &+ \left(D_{23}B_{23}^{-1}A_{23} - C_{23}\right)\mathbf{v}_3^{-}\delta t_3^{-} \end{aligned} \tag{45}$$

Using Eqs. (43) and (45), and noting the fixed constraints $\mathbf{r}_2^- = \mathbf{r}_2^+$, $t_2^- = t_2^+$, and the relation $C_{k-1,k} - D_{k-1,k}B_{k-1,k}^{-1}A_{k-1,k} = B_{k-1,k}$, the variation in $\Delta\mathbf{V}$ at Target Point 2 due to variations in the control variables i.e. target point positions and time, can be written as

$$\delta\Delta\mathbf{v}_2 = \delta\mathbf{v}_2'^{+} - \delta\mathbf{v}_2'^{-} = \begin{bmatrix} M_1^2 & M_{t1}^2 & M_2^2 & M_{t2}^2 & M_3^2 & M_{t3}^2 \end{bmatrix} \begin{bmatrix} \delta\mathbf{r}_1'^{+} \\ \delta t_1^+ \\ \delta\mathbf{r}_2' \\ \delta t_2 \\ \delta\mathbf{r}_3'^{-} \\ \delta t_3^- \end{bmatrix} \tag{46}$$

where

$$\begin{aligned} M_1^2 &= -C_{21} + D_{21}B_{21}^{-1}A_{21} \\ M_{t1}^2 &= \left(C_{21} - D_{21}B_{21}^{-1}A_{21}\right)\mathbf{v}_1^+ \\ M_2^2 &= D_{23}B_{23}^{-1} - D_{21}B_{21}^{-1} \\ M_{t2}^2 &= \mathbf{a}_2^+ - D_{23}B_{23}^{-1}\mathbf{v}_2^+ - \mathbf{a}_2^- + D_{21}B_{21}^{-1}\mathbf{v}_2^- \\ M_3^2 &= C_{23} - D_{23}B_{23}^{-1}A_{23} \\ M_{t3}^2 &= \left(D_{23}B_{23}^{-1}A_{23} - C_{23}\right)\mathbf{v}_3^- \end{aligned}$$

Similar to the above equation, the differential correction for the other target points can also be easily derived. If the total number of the target points is *N* then *N*-2 differential correction equations analogous to Eq. (46) are needed for each of the interior target points, and all these equations can be assembled into a single system of linear equations as

$$\begin{bmatrix} \delta\Delta\mathbf{v}_2 \\ \delta\Delta\mathbf{v}_3 \\ \vdots \\ \delta\Delta\mathbf{v}_{N-1} \end{bmatrix} = \begin{bmatrix} M_1^2 & M_{t1}^2 & M_2^2 & M_{t2}^2 & M_3^2 & M_{t3}^2 & 0 & \cdots & 0 \\ 0 & 0 & M_2^3 & M_{t2}^3 & M_3^3 & M_{t3}^3 & M_4^3 & \cdots & 0 \\ \vdots & \vdots & \vdots & \vdots & \vdots & \vdots & \vdots & \ddots & \vdots \\ 0 & 0 & \cdots & M_{N-2}^{N-1} & M_{t(N-2)}^{N-1} & M_{N-1}^{N-1} & M_{t(N-1)}^{N-1} & M_N^{N-1} & M_{tN}^{N-1} \end{bmatrix} \begin{bmatrix} \delta\mathbf{r}_1^+ \\ \delta t_1^+ \\ \delta\mathbf{r}_2 \\ \delta t_2 \\ \delta\mathbf{r}_3 \\ \delta t_3 \\ \vdots \\ \delta\mathbf{r}_N^- \\ \delta t_N^- \end{bmatrix} \quad (47)$$

The above system of under-determined linear system of equations is solved using the minimum norm solution as in Eq. (41). The corrections are then applied to the position and time of each of the *N* target points. The Level-2 corrections reduce the magnitude of each velocity discontinuity but will introduce a small position discontinuity as a result when each segment is propagated again. Therefore, after Level-2 corrections are applied, Level-1 corrections are computed again. This cycle is repeated for five to six times until all the position and velocity discontinuities are below the tolerance levels. It should be noted that the Level-2 differential correction does not reduce the velocity discontinuity between the first and the last target points, and, moreover, it displaces the first and last target points from the initial states. As a result, a fully periodic starting solution will gradually become non-periodic as a result of the position and velocity discontinuity between the first and the last target points introduced by the two-level differential correctior. Additional constraints are added to the Level-2 differential corrector to mitigate this limitation.

3.3.2. Periodicity Constraints. To find a periodic halo orbit in the ER3BP near small bodies using the two-level differential corrector, a periodic starting solution such as a halo orbit from the CR3BP can be chosen and divided into four segments with five target points. To prevent the position and velocity discontinuities between the first and the last target points to increase during the correction process, the Level-2 corrections need to be modified to introduce additional constraints to enforce the continuity between the first and the last target point. Marchand *et al.* proposed an approach where the periodicity constraints are modeled as algebraic constraints and added to the Level-2 corrections Eqn. (47) [22]. This constraint is defined as

$$\alpha = \begin{bmatrix} \mathbf{r}_1^+ - \mathbf{r}_N^- \\ \mathbf{v}_1^+ - \mathbf{v}_N^- \end{bmatrix} \tag{48}$$

The above constraint is a target variable whose value needs to be reduced to zero during the correction process as

$$\delta\alpha = -\alpha = \begin{bmatrix} -\left(\delta\mathbf{r}_1^+ - \delta\mathbf{r}_N^-\right) \\ -\left(\delta\mathbf{v}_1^+ - \delta\mathbf{v}_N^-\right) \end{bmatrix} \tag{49}$$

In the above equation, the dependence of the target variables $\delta\mathbf{v}_1^+$ on the control variables can be written using Eq. (42) and similarly for the target variable $\delta\mathbf{v}_N^-$ using the variational equation for the last trajectory segment. The final differential correction for the periodicity constraint can be written as

$$\delta\alpha = \begin{bmatrix} \delta\mathbf{r}_1^+ - \delta\mathbf{r}_N^- \\ -B_{21}^{-1}A_{21}\delta\mathbf{r}_1^+ + \left(\mathbf{a}_1^+ + B_{21}^{-1}A_{21}\mathbf{v}_1^+\right)\delta t_1^+ + B_{21}^{-1}\delta\mathbf{r}_2 - B_{21}^{-1}\mathbf{v}_2^-\delta t_2 - \\ B_{N-1,N}^{-1}\delta\mathbf{r}_{N-1} + B_{N-1,N}^{-1}\mathbf{v}_{N-1}^+\delta t_{N-1} + B_{N-1,N}^{-1}A_{N-1,N}\delta\mathbf{r}_N^- - \left(\mathbf{a}_N^- + B_{N-1,N}^{-1}A_{N-1,N}\mathbf{v}_N^-\right)\delta t_N^- \end{bmatrix} \quad (50)$$

The above constraint equation is appended to the Level-2 system of equations Eq. (47) and a minimum-norm solution is computed for this underdetermined system. It was observed that for the Sun-small body systems considered in this work, the above periodicity constraint was too stringent and the two-level differential corrector did not converge when periodicity constraints were used. It is suspected that the reason for the divergence of the two-level differential corrector is that a 3-D periodic orbit close to the chosen target points may not exist in this region, or is at least difficult to identify with current analytical and numerical techniques. For verification that the two-level differential corrector was able to find a periodic halo orbit (in general cases), the two-level differential corrector with the above periodicity constraints was applied to a known 3-D periodic orbit using the Earth-Moon system mass ratio with a "high" eccentricity of 0.3. The initial conditions for this periodic orbit were found using the differential corrector first proposed by Broucke [9] and used by Campagnola *et al.* [19] to find halo orbits in the Earth-Moon system. These initial conditions, when propagated for exactly one halo orbit period using the LP-centric EOMs for the ER3BP given in Section 2.4, produce an orbit that has position and velocity discontinuity of 4,357 km and 28.5 m/s between the initial and final state. Figure 3.3 shows this integrated orbit in the Earth-Moon system (with eccentricity 0.3). It is noted that this orbit is displaced from the L_2 libration point toward the Moon as most resonant initial conditions required by Broucke's differential corrector are found in this region as noted by Howell [18]. The reason for the

large discontinuity is likely due to the different forms of the EOMs used by Broucke's differential corrector [9], which has true anomaly of the primaries as the independent variables and the EOMs used in the two-level differential corrector in this work has time as the independent variable. Nevertheless, the shape of the orbit is retained when propagated using the LP-centric EOMs. The orbit shown in Figure 3.3 is divided into eight segments and then the two-level differential corrector augmented with position and velocity constraints, was applied. The two-level differential corrector converged in this case and the position and velocity discontinuities at each of the target point after the corrections were applied are shown in Figure 3.4. The corrected orbit is shown in Figure 3.5. It is noted that the Level-2 differential corrector was able to reduce the velocity discontinuity between the first and last target point from 28.5 m/s to 0.002 m/s for the Earth-Moon halo orbit with negligible position discontinuity.

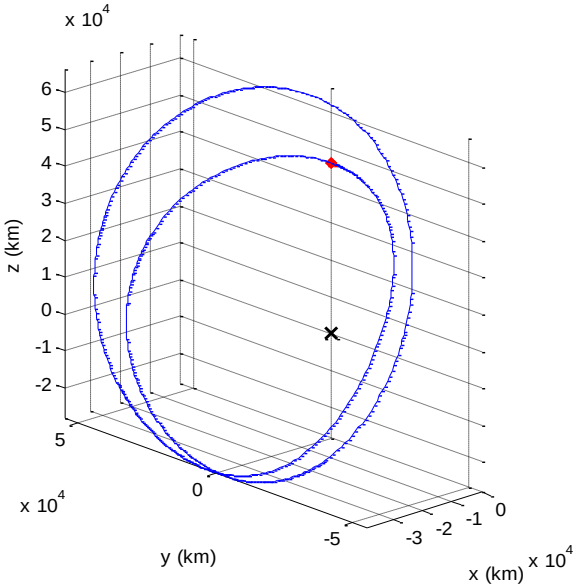

Figure 3.3. An L_2 Halo Orbit in the Earth-Moon System with Eccentricity 0.3.

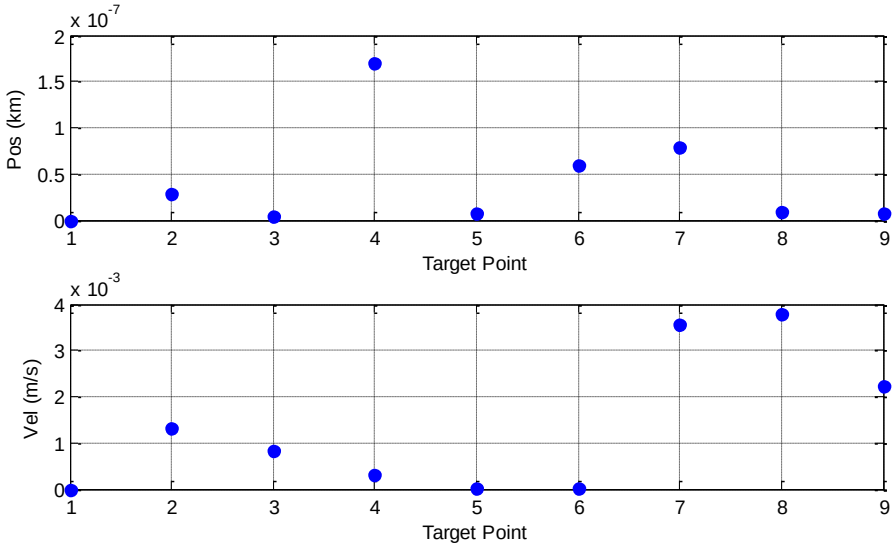

Figure 3.4. Position and Velocity Discontinuities after Six Iteration of the Two-Level Differential Corrector for the Earth-Moon L_2 Halo Orbit with Eccentricity 0.3.

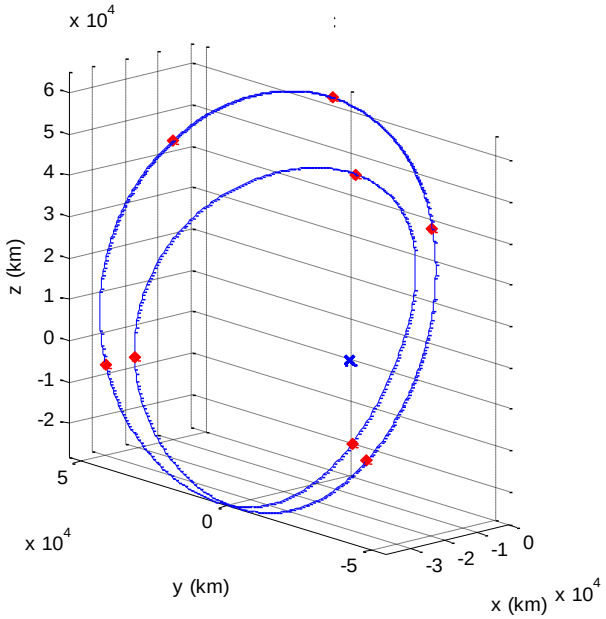

Figure 3.5. Corrected L_2 Halo Orbit in the Earth-Moon System with Eccentricity 0.3 Using the Two-Level Differential Corrector.

In the Sun-small body system, a position-only constraint was added to the two-level differential corrector to avoid divergence. This position-only constraint enforces the condition $\delta\mathbf{r}_1^+ = \delta\mathbf{r}_N^-$ by adding the constraints specified by the matrix M_N^{N-1} from the last segment variation equation on to the first target point. This is accomplished by moving the position of the matrix M_N^{N-1} to the first three columns of the last row of the state relationship matrix in Eq. (47). The Level-2 corrections computed for the first target points are also applied to the last target points in this case.

3.4. RESULTS

Many halo orbits computed in the CR3BP were numerically continued in the ER3BP using the two-level differential corrector for a number of small bodies chosen from Table 3.1. The resulting orbits in the Sun-small body ER3BP system are presented in this section. Using the results from Section 3.2 a number of halo orbits were first computed in the CR3BP for different small bodies in the Sun-SSSB system. To numerically continue these orbits into the ER3BP, two revolutions of the halo orbits were assembled and divided into eight segments with nine target points. Because in the CR3BP the halo orbits are perfectly periodic, the second revolution of the halo orbit was taken exactly same as the first revolution. Before the numerical continuation was attempted, all the target points were translated into the LP-centric frame using the transformations described in Section 2. It was found that the numerical integrations in the LP-centric frame were more accurate than those using the barycentric frame due to the smaller magnitude of the *x* coordinate and the fewer number of coordinate transformations

involved. For instance, in the barycentric frame a numerical continuation from eccentricity value 0.0 to 0.1 took 300 steps compared to only 10 steps when the integration was performed using the LP-centric frame. During the numerical continuation, the two-level differential corrector was used iteratively to reduce the position and velocity discontinuities between the segments. It was observed that with the increase in the eccentricity, the velocity discontinuity between the first and the last target point gradually increases in spite of the periodicity constraint used. Two small bodies from the Table 3.1 *viz. 433 Eros* and *1 Ceres* were chosen and halo-like orbits were computed near them using the two-level differential corrector. The *MATLAB* ode113 integrator was used to integrate orbits in both systems with the relative tolerance taken as 10^{-13}.

3.4.1. The Sun-*433 Eros* System. An L_2 halo-like orbit computed for the Sun-433 Eros system in the ER3BP with eccentricity 0.2229 is shown in Figure 3.6 and Figure 3.7. The orbit was continued from the two revolutions of the halo orbit in the CR3BP divided into a total of eight segments. The position and velocity discontinuity magnitudes at each target points after Level-1 and Level-2 corrections are shown in Figure 3.8. All the position and velocity discontinuities were reduced to less than 0.15 cm and 0.4 nanometers per second after six iterations of Level-1 and Level-2 corrections. The position-only constraint was used as described in the previous section. The velocity discontinuity between the first and the last target point was 0.015 m/s. If a mission design requires multiple revolutions in this orbit, then this discontinuity can significantly increase the station-keeping costs if chosen as a nominal orbit. To reduce this cost, a similar orbit can be computed near 433 Eros by continuation of as many revolutions of

the CR3BP halo orbits as required into the ER3BP as shown in Section 5.3. A 3-D plot of the L2 halo-like orbit for the Sun-433 Eros system is shown in Figure 3.9 drawn to scale.

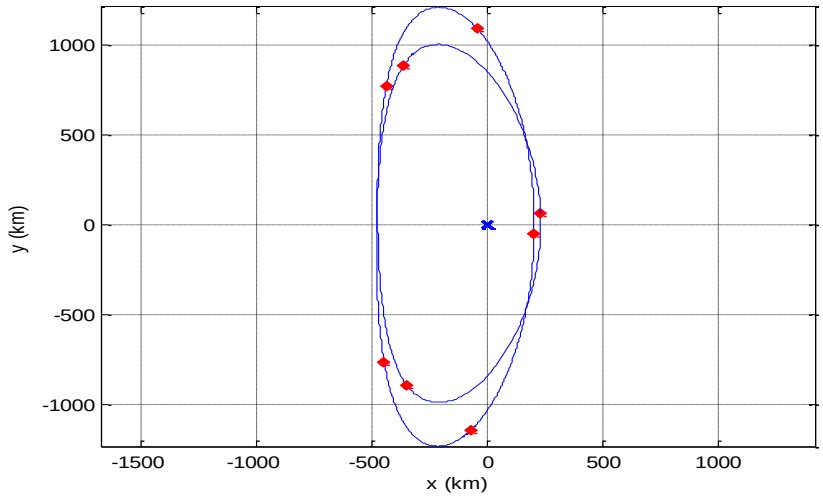

Figure 3.6. X-Y Projection of L_2 Halo-Like Orbit in the Sun-*433 Eros* System with Eccentricity 0.2229.

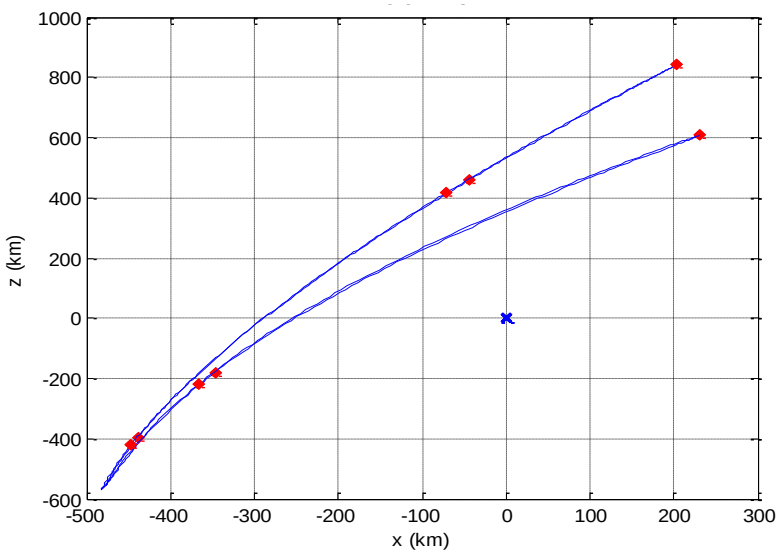

Figure 3.7. X-Z Projection of L_2 Halo-Like Orbit in the Sun-*433 Eros* System with Eccentricity 0.2229.

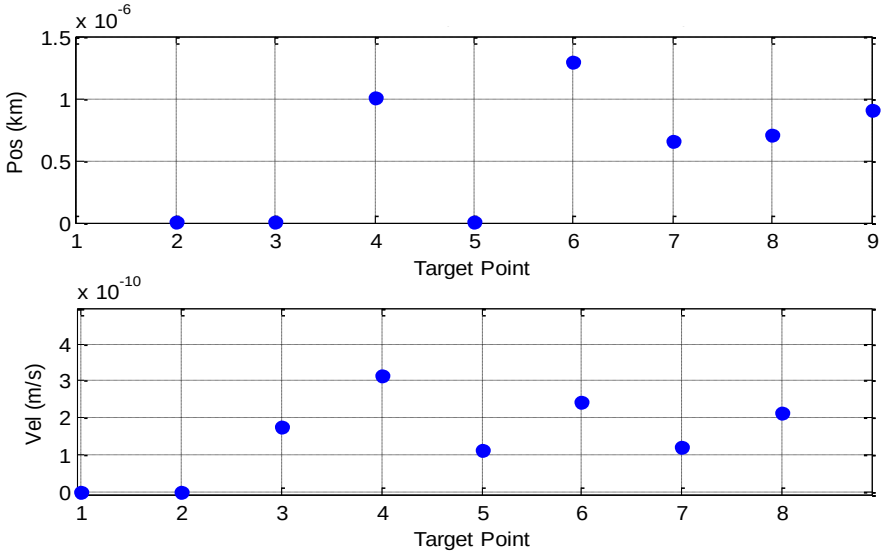

Figure 3.8. Position and Velocity Discontinuities after Six Iterations of the Two-Level Differential Corrector.

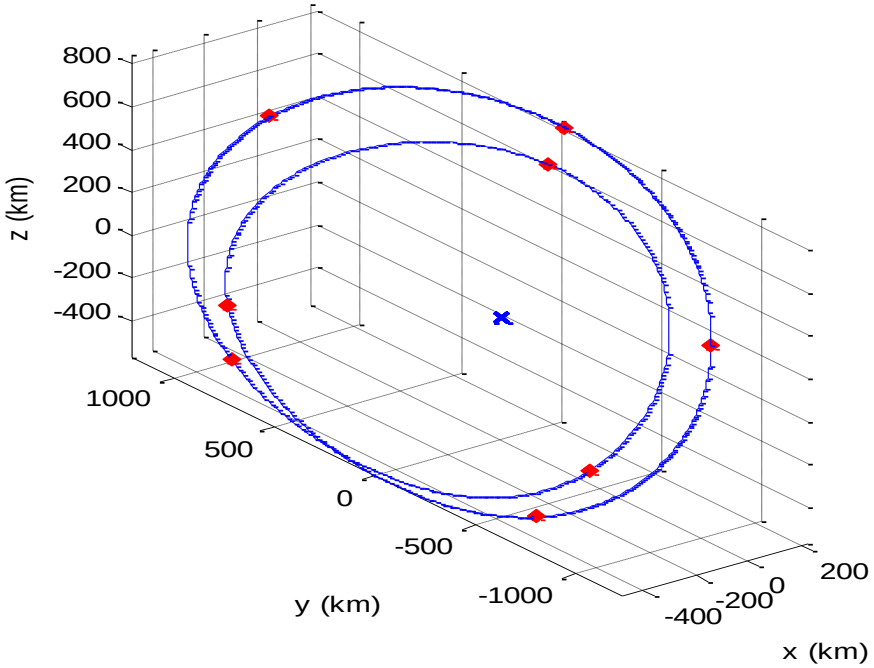

Figure 3.9. L_2 Halo-Like Orbit Drawn to Scale with Target Points in the Sun-*433 Eros* System with Eccentricity 0.2229.

3.4.2. The Sun-*4 Vesta* System. Similar to the method employed for *433 Eros*, an L_1 halo orbit in the CR3BP for the Sun-*4 Vesta* system was numerically continued into the ER3BP with eccentricity 0.0895 using the two-level differential corrector. The periodicity constraint was only applied to position continuity. Figure 3.10 and Figure 3.11 show the resulting halo-like orbit near *4 Vesta*. The position and velocity discontinuities are shown in Figure 3.12. Six iterations of Level-1 and Level-2 differential corrections were used during each step of the numerical continuation in eccentricity. The velocity discontinuity between the first and the last target point was 0.31 m/s. A 3-D plot with the orbit drawn to scale is shown in Figure 3.13.

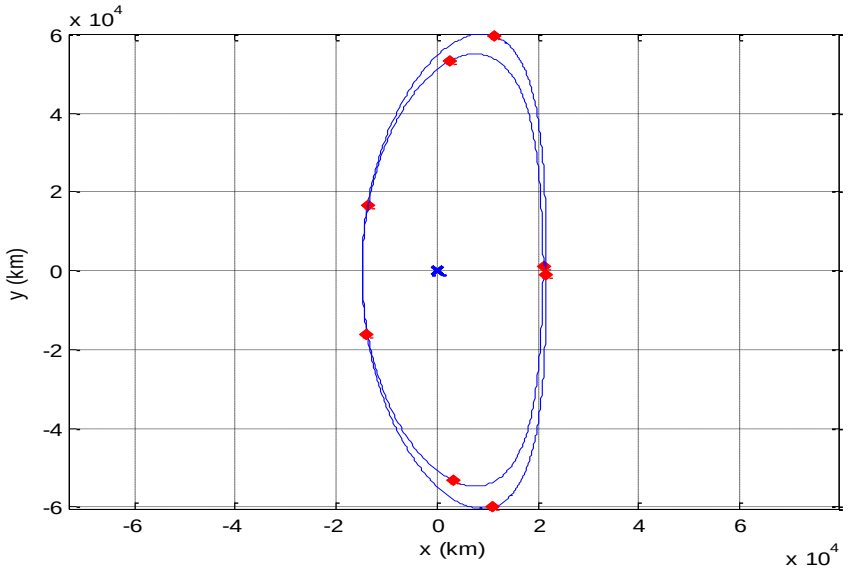

Figure 3.10. L_1 Halo-Like Orbit with Target Points in the Sun-*4 Vesta* System with Eccentricity 0.0895.

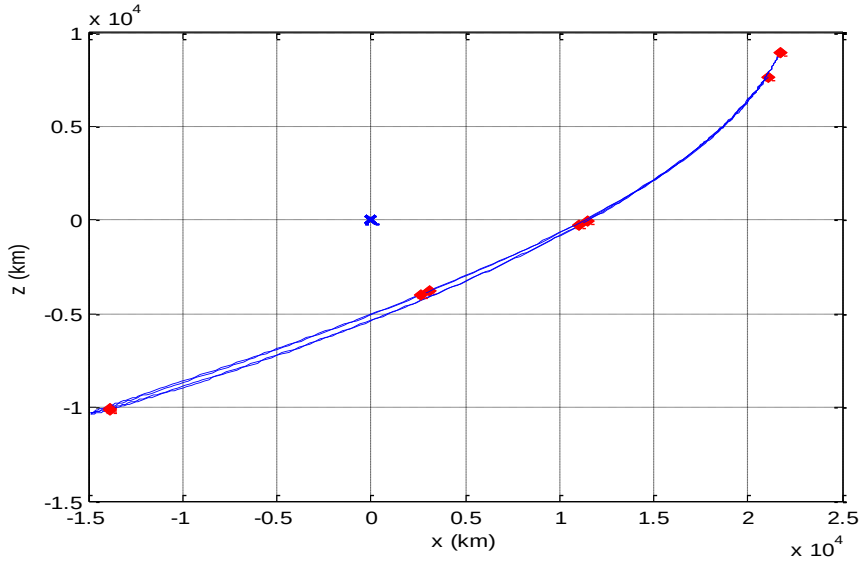

Figure 3.11. L_1 Halo-Like Orbit with Target Points in the Sun-*4 Vesta* System with Eccentricity 0.0895.

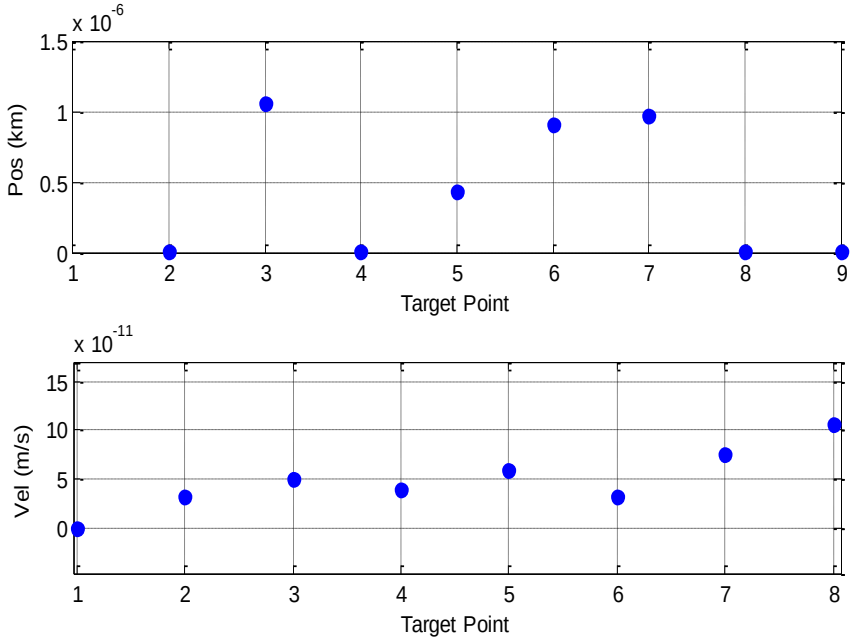

Figure 3.12. Position and Velocity Discontinuities After Six Iterations of the Two-Level DC in the Sun-*4 Vesta* System.

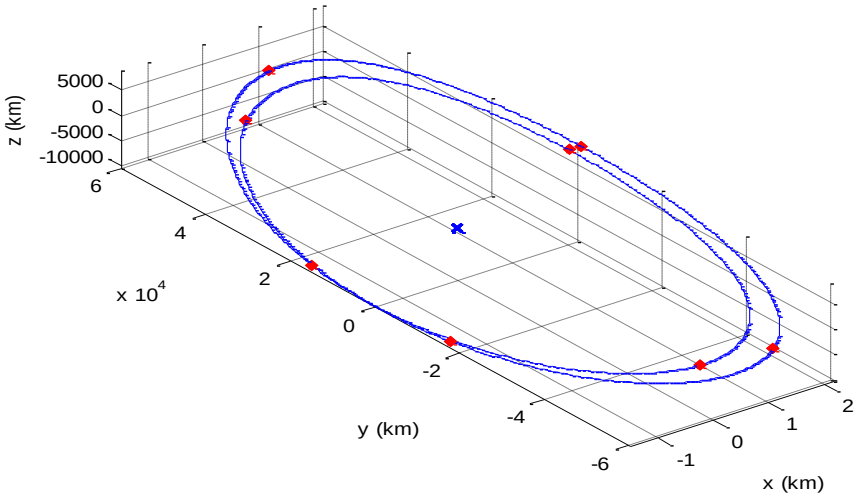

Figure 3.13. L_1 Halo-Like Orbit Drawn to Scale with Target Points in the Sun-*4 Vesta* System with Eccentricity 0.0895.

4. STABILITY ANALYSIS

In the previous chapter, three-dimensional halo orbits were computed near bodies as small as asteroid *1999 AO10* in the CR3BP. In the ER3BP, the two-level differential corrector was used to compute halo-like orbits near a few small bodies with significant eccentricity. These orbits are not exactly periodic in the ER3BP as there is small discontinuity in velocity between the first and the last target points as discussed in the previous chapter. Despite the presence of the velocity discontinuity, these quasi-periodic orbits can be successfully used as nominal orbits for station-keeping as is discussed in the Section 5. The cost of station-keeping about these nominal orbits in the presence of uncertainties, however, depends upon the stability characteristics of these orbits. In this chapter, the stability of the nominal orbits computed in the previous chapter is analyzed using Floquet theory. It is known that the orbits around collinear libration points are unstable in the ER3BP for all values of mass ratios and eccentricity [6]. The extent of the instability is important because it directly affects the station-keeping costs for maintaining a spacecraft in the reference orbits. The magnitude of instability of a periodic orbit around a collinear libration point in the first-order sense can be assessed using Floquet analysis.

4.1. FLOQUET ANALYSIS

It is known that the eigenvalues of the monodromy matrix computed along a periodic orbit in the ER3BP occur in reciprocal pairs as μ and $1/\mu$ and two of them are *not* unity in contrast to the case for the CR3BP, in which one pair of eigenvalues is unity.

Floquet analysis is used in this work to assess the linear stability of the halo-like orbits in the elliptic Sun-small body system. The linear stability of a periodic orbit can be analyzed using the variation equations of the system given as

$$\dot{\phi}(t,t_0) = A(t)\phi(t,t_0); \phi(t_0,t_0) = I \tag{51}$$

where the *A(t)* matrix is the Jacobian matrix of the ER3BP differential equations and ϕ is the STM. If ω is the period of one revolution of the periodic orbit, then the above equation can be numerically integrated for one complete revolution of the orbit to obtain the monodromy matrix *M* as

$$M = \phi(t_0 + \omega, t_0) \tag{52}$$

According to Floquet theory, a linear time-varying (LTV) homogeneous system can be converted into an equivalent linear time-invariant (LTI) system with the eigenvalues of the new LTI system related to the eigenvalues of the monodromy matrix of the LTV system through [37]

$$\lambda = e^{\alpha\omega} \tag{53}$$

where λ is an eigenvalue of the monodromy matrix and α is the corresponding eigenvalue of the equivalent LTI system, often called the "characteristic exponent." It should be noted that the linearized ER3BP dynamics form an LTV system (due to nonautonomous

periodic motion of the primaries in their elliptic orbits). A periodic orbit is stable in the linear sense if the real parts of all the characteristic exponents are less than or equal to zero. In a Hamiltonian system, however it is not possible for all the real parts of all the characteristic exponents to be negative. As a result the real parts must all vanish in order to identify a stable periodic orbit. Equivalently, this means that all the eigenvalues must lie on the unit circle. Scheeres and Marzari [24] used the characteristic time associated with a periodic orbit about an equilibrium point to assess its stability in a Sun-comet system with solar radiation pressure and the comet's orbit eccentricity effects included. Here, the effects of the extremely small mass of the smaller primary on the eigenvalues of the monodromy matrix and thus on the stability of the halo-like orbits are considered.

4.2. RESULTS

In this section, the results pertaining to stability of the halo-like orbits computed in the Sun-small body ER3BP systems are analyzed. Although the halo-like orbits computed using the two-level differential corrector are not precisely periodic, it was observed that the eigenvalues of the monodromy matrix for these orbits still retain the reciprocal form (though not exactly). In general, eigenvalues farther away from the unit circle are "more" unstable and thus will incur higher station-keeping costs. In other words, an increase in the magnitude of the real part of the characteristic exponent will increase the instability of the orbit. Figure 4.1 shows a plot of the eigenvalues of the monodromy matrix for one revolution of the halo-like orbit in the Sun-*433 Eros* ER3BP system with eccentricity 0.2229. It should be noted that the two revolutions of the halo

orbit in the CR3BP when continued into the ER3BP is considered as a single revolution of the halo-like orbit. As expected two of the eigenvalues are real and the other four are complex numbers. The four complex eigenvalues were very close to the unit circle as shown in the figure and thus are stable. Of the two real eigenvalues, one has magnitude greater than one and the other smaller. These eigenvalues make the orbit unstable. To compare the instability magnitude, the characteristic exponents for these orbits were computed using Eq. (53). For the Sun-*433 Eros* system the two characteristic exponents corresponding to the two real eigenvalues are 10.254×10^{-3} and -10.224×10^{-3} in nondimensional units. The reciprocal of these values gives the time constant which governs how fast the spacecraft diverges from these reference orbits. The small magnitude of these unstable characteristic exponents shows that the level of instability of these orbits is small.

The eigenvalues corresponding to the L_1 orbit for the Sun-4 Vesta ER3BP system with eccentricity 0.01895 are shown in Figure 4.2. The characteristic exponents corresponding to the two real eigenvalues are found to be 3.654×10^{-3} and -3.653×10^{-3}. It should be noted that the eccentricity of *4 Vesta* is much smaller than that of *433 Eros,* which plays a role in observing a smaller instability in the case of the halo-like orbits near *4 Vesta*. Bennett has shown that in the ER3BP the instability of the collinear libration points increases with eccentricity for all values of the mass ratio [6].

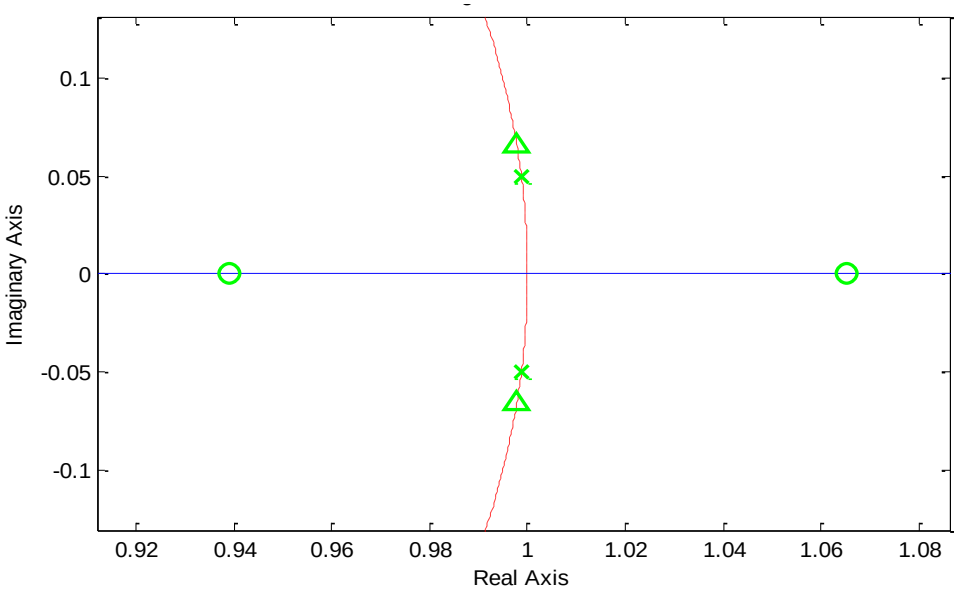

Figure 4.1. Eigenvalues of the Monodromy Matrix of the L_2 Halo-Like Orbit in the Sun-*433 Eros* System with Eccentricity 0.2229. The Red Dashed Line Shows the Unit Circle.

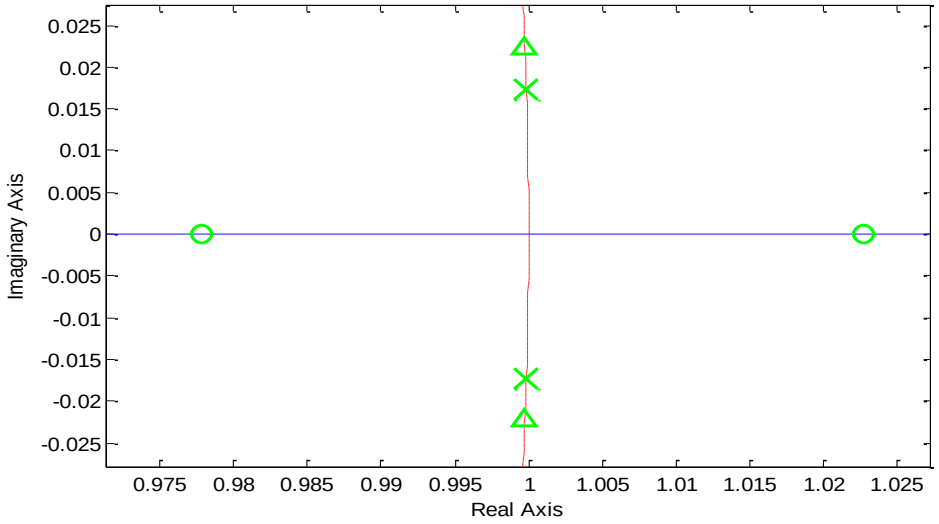

Figure 4.2. Eigenvalues of the Monodromy Matrix of the L_1 Halo-Like Orbit in the Sun-*4 Vesta* System with Eccentricity 0.0895. The Red Dashed Plot Shows the Unit Circle.

5. STATION-KEEPING OF LIBRATION POINT ORBITS NEAR SMALL BODIES

The method used to compute halo-like three-dimensional libration point orbits in the vicinity of the small bodies presented in Section 3, can be used to design reference orbits meeting mission requirements. The dynamical models used for computing the reference orbits generally lack some perturbative accelerations such as nonspherical gravity, solar radiation pressure (SRP), third-body gravitational effects, etc. The collinear libration point orbits are unstable in the linear as well as nonlinear sense [2]. In the previous chapter it was seen that the reference orbits computed in Section 3 using the two-level differential corrector are unstable in the linear sense; with the instability magnitude indicated by the magnitude of their characteristic exponents. Therefore station-keeping is required to maintain a spacecraft near these reference orbits. The station-keeping costs in terms of ΔV can be prohibitively high if the mode used to define the reference orbits does not adequately represent the actual dynamics. The two-level differential corrector algorithm discussed in Section 3 can be used to find reference orbits in a high fidelity ephemeris-based model, which can reduce ΔV costs. However, the known dynamic models of the modeled forces have significant structured as well as unstructured uncertainties. In the case of SSSBs such as asteroids and comets, there are additional uncertainties in the knowledge of their physical as well as orbital characteristics. As a result, robust methods that can accommodate significant uncertainties in the dynamic model are needed for effective station. It should be noted that these libration orbits are small in size and are located close to the small bodies compared to analogous orbits found near bodies such as the Earth or Moon.

In this section a robust nonlinear sliding mode controller is designed for station-keeping of libration point orbits near small bodies. It is shown that this low-thrust controller is robust to the tracking errors, thruster bun errors, and uncertainties in the dynamic model. The next section discusses the specific challenges for station-keeping of small libration point orbits near small bodies. The following sections discuss the sliding mode controller design. A *MATLAB*-based simulation was developed that incorporates various perturbations as discussed in Section 5.3. The last section presents the results for station-keeping of halo-like orbits near small bodies.

5.1. CHALLENGES FOR STATION-KEEPING

Missions to SSSBs tend to be more challenging because of the limited knowledge regarding their physical and orbital properties. The missions sent to the libration point orbits of Sun-Earth system such as ISEE-3 and SOHO have larger error margins that can be tolerated without endangering the mission. This is not always the case, especially for a human mission destined for regions near small bodies. The error margins are smaller due to the smaller size of the orbits and their close proximity to the surface of the small body.

5.1.1. Libration Point Orbit Size and Location. The distance of libration point locations from the small body and size of the orbits about these points are shown in Section 3 for various small bodies. The collinear libration points range from 5 km to a body like *1999 AO10* with a diameter of approximately 100 m to 218,000 km for the L_1 for *1 Ceres* dwarf planet distance with a diameter of 900 km (assuming 1 AU as their semimajor axes). These distances are much smaller than the distance of the collinear

libration points found in the Earth-Moon or Sun-Earth system (e.g., 1.495×10^6 km for the L_1 distance in the Sun-Earth system). Moreover, a spacecraft in a libration point orbit comes closer to the surface of the small body based on the size of the orbit. For *1999 AO10* the minimum *x* amplitude was found to be 0.7 km for an L_1 halo orbit, and for 4 Vesta the minimum *x* amplitude was found to be 30,000 km. These are the minimum values and thus larger orbits do exist. Due to the close proximity of libration point locations to the small body, it is likely to be necessary to "tightly" control the spacecraft orbits near small bodies with smaller error margins.

5.1.2. Uncertainties in Physical and Orbital Properties. The knowledge of size, mass, orbit, rotational axis and rotational rate of SSSBs is limited. Any station-keeping controller designed to maintain the spacecraft on the nominal orbits must be robust to the significant uncertainties present in the nominal dynamic model used to compute the reference orbits. It should be noted that the inaccuracies in the mass estimate of the small body affects the location as well as size of libration point orbits used as the reference orbits.

5.1.3. Other Perturbations. The other perturbations that can increase the station-keeping costs include the solar radiation pressure and third-body perturbation effects that are not accounted for in computing the nominal solutions.

5.2. SLIDING MODE CONTROL

This section introduces the sliding mode control (SMC) design which is a nonlinear controller that is robust to uncertainties present in the dynamic model provided

an upper bound on the uncertainty is known. Reference [38] gives a detailed explanation of SMCs. Here a brief description is provided related to the problem of station-keeping of a libration point orbit. Consider a two state nonlinear system as

$$\begin{aligned} \dot{x}_1 &= x_2 \\ \dot{x}_2 &= f(x_1, x_2) + u \end{aligned} \tag{54}$$

The objective is to compute the control signal u to track a desired state x_d. The sliding mode design principle is to force the system using control to follow a lower order system called a sliding surface. A typical sliding surface for the above tracking system can be given as

$$s = ae + \dot{e} \tag{55}$$

where

$$e = x_1 - x_d$$

The symbol s is the sliding surface and a is a positive constant that determines how fast the system state x_1 converges to the desired state x_d. Using the sliding surface the tracking problem is transformed to a problem of remaining on the sliding surface s. In other words, $e = 0$ is a unique solution of the equation $s = 0$. The second order tracking problem has been converted to a first order finite-time regulator problem in s. Additionally the bound on s is directly related to the bound on the error e. The system

motion in the sliding mode can be interpreted as an average of the system dynamics on both sides of the surface [38]. Assuming the exact dynamics of the system are known, an equivalent control can be computed which is a continuous component of the total control signal that ensures $\dot{s} = 0$; in other words the tracking error goes to zero. This equivalent control component can be computed as

$$\dot{s} = 0 \tag{56}$$

or

$$a\dot{e} + f(x_1, x_2) + u_{eq} = 0 \tag{57}$$

Solving for the control using the above equation, an expression for the equivalent control is found as

$$u_{eq} = -a\dot{e} - f(x_1, x_2) \tag{58}$$

or

$$u_{eq} = -ax_2 + a\dot{x}_d - f(x_1, x_2) \tag{59}$$

The equivalent control u_{eq} will maintain the system in the sliding mode only if the system is initially in the sliding mode and the exact system dynamics are known. These two

conditions are generally not met and a discrete control component is added to the equivalent control computed above in order to bring the system into the sliding mode despite of the uncertainties present in the known dynamics. However, an upper bound on the uncertainty must be known in order to design this discrete control component. The discrete control component is given as

$$u_{disc} = \eta \, sign(s) \tag{60}$$

where η is a parameter that determines the finite time the system takes to reach the sliding mode and *sign* is the regular sign function. The value of the η can be computed using the Lyapunov stability theorem. A Lyapunov function for stability analysis is chosen as

$$V = \frac{1}{2} s^2 \tag{61}$$

The above function can be differentiated to yield

$$\begin{aligned} \dot{V} &= s\dot{s} \\ \dot{V} &= s\left(ax_2 - a\dot{x}_d + f(x_1, x_2) + u\right) \end{aligned} \tag{62}$$

Substituting the value of the control as sum of equivalent and discontinuous control components, the above equation can be written as

$$\begin{aligned}\dot{V} &= s\left(ax_2 - a\dot{x}_d + f(x_1, x_2) - ax_2 + a\dot{x}_d - f_n(x_1, x_2) - \eta\, sign(s)\right)\\ \dot{V} &= s\left(f(x_1, x_2) - f_n(x_1, x_2)\right) - \eta\, s\, sign(s)\\ \dot{V} &= s\left(f(x_1, x_2) - f_n(x_1, x_2)\right) - \eta|s|\end{aligned} \tag{63}$$

where f_n represents the known nominal dynamics. If the difference between the actual system dynamics and the known nominal dynamics is assumed known, $\dot{V}$ can be made negative definite as

$$\dot{V} < -\eta|s| \text{ if } \eta = F + K \tag{64}$$

where

$$\left|f(x_1, x_2) - f_n(x_1, x_2)\right| < F \tag{65}$$

In the above equation K is the parameter that determines the finite time the system takes to reach the sliding mode from a given initial state. It should be noted that the system dynamics f and f_n can be a function of time or some other variable external to the system. The sliding mode control formulation derived above has a discontinuous control component which might result in high frequency switching actions when the system is operating in a region very close to the sliding mode. To avoid this chattering behavior, a saturation function can be used in the above formulation as opposed to the sign function [39].

5.3. STATION-KEEPING CONTROLLER

In this section, the station-keeping controller is designed using the sliding mode control theory given in the previous section for the libration point orbits. The nominal dynamic model chosen for designing the equivalent control is the ER3BP. The controller is designed to compensate for the perturbation effects from SRP, tracking error, and maneuver burn errors as explained in the following section.

5.3.1. Reference Orbit. The reference orbits are designed as per the mission requirements and computed offline prior to launch of the actual mission. These orbits provide the desired states given a time instant, which are used by the station-keeping controller to compute the required control signal to apply. The halo-like orbits computed in Section 3 are used as the reference orbits for the SMC controller in this work. It was seen in the Section 3 that these nominal orbits have a velocity discontinuity between the first and the last target point. This velocity discontinuity can increase the station-keeping costs if mission duration requires multiple revolutions of the reference orbit. To avoid this cost, multiple revolutions of the halo orbits in the CR3BP spanning the entire duration of the mission for a Sun-SSSB system are corrected using the two-level differential corrector. In this study, six revolutions of the CR3BP halo orbits were chosen to compute the reference orbits in the ER3BP. These reference orbits were stored as cubic splines using the *MATLAB* software. The station-keeping controller used the stored reference orbit data to interpolate the desired states at a given time in order to compute the required control. Figure 5.1 shows the six revolutions of a halo-like orbit in the Sun-*433 Eros* system with eccentricity 0.2229. The velocity discontinuity between the first and the last target point in this case was found to be 0.08 m/s, however the entire nominal

orbit spanning five Earth years was completely continuous in position as well as in velocity as shown in Figure 5.2.

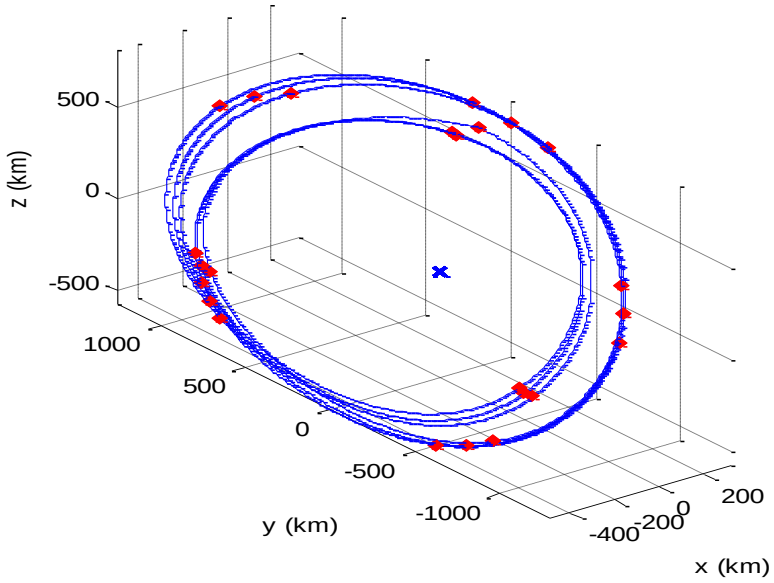

Figure 5.1. L_2 Halo-Like Reference Orbit in the Sun-*433 Eros* System with Eccentricity 0.2229.

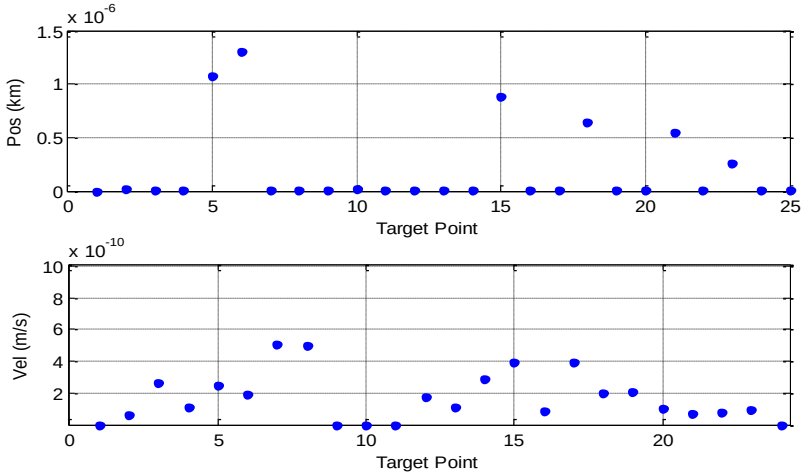

Figure 5.2. Position and Velocity Discontinuities for the Sun-*433 Eros* Halo-Like Reference Orbit.

5.3.2. Sliding Mode Control Design. In terms of modern control terminology, the ER3BP model is a Multi-Input Multi-Output (MIMO) system. The theory developed in the previous section for Single-Input Single-Output (SISO) can easily be extended to the MIMO systems as shown in this section. The sliding surface or manifold for the ER3BP system can be designed using Eq. (55) as

$$\begin{aligned} s_i &= a_i e_i + \dot{e}_i,\ i = 1,2,3 \\ e_i &= x_i - \left(x_d\right)_i,\ i = 1,2,3 \end{aligned} \tag{66}$$

where the subscript *i* represents the three coordinates of the current spacecraft position *x* and the desired state from the nominal orbit x_d. The objective is to make the error *e* go to zero. The sliding mode control vector to bring the system to the sliding manifold and maintain it there can be computed in this case as

$$u_i = -a_i \dot{x}_i + a_i.\left(\dot{x}_d\right)_i - f_{ni}(t, \mathbf{X}) - \eta_i sign(s_i),\ i = 1,2,3 \tag{67}$$

where

$$\mathbf{X} = \begin{bmatrix} x & y & z & \dot{x} & \dot{y} & \dot{z} \end{bmatrix}^T$$

In the above equation, **X** is the state vector consisting of six states of the spacecraft, x_i is an element of the current state vector **X**, which is typically provided by an estimator like the Extended Kalman Filter, and x_d is the nominal or desired orbit state element that is

computed before the mission launches. The SMC controller parameters a_i and η_i are the parameters whose values are chosen based on the uncertainty level expected in the nominal dynamics and how fast the system is expected to converge to the desired states. The next subsection describes how these parameter values are chosen for the SMC station-keeping controller for libration point orbits in this work. The nominal dynamic term f_{ni} represents the ER3BP dynamics as discussed in Chapter 2 and is given as

$$\begin{aligned}
\left(f_n\right)_1 &= +2\dot{\theta}\dot{y} - \ddot{\theta}y + \dot{\theta}^2 x - \left(\frac{(1-\mu)(x+\mu)}{\|\mathbf{r}_1\|^3} + \frac{\mu(x-1+\mu)}{\|\mathbf{r}_2\|^3}\right) \\
\left(f_n\right)_2 &= -2\dot{\theta}\dot{x} - \ddot{\theta}x + \dot{\theta}^2 y - \left(\frac{(1-\mu)y}{\|\mathbf{r}_1\|^3} + \frac{\mu y}{\|\mathbf{r}_2\|^3}\right) \\
\left(f_n\right)_3 &= -\left(\frac{(1-\mu)z}{\|\mathbf{r}_1\|^3} + \frac{\mu z}{\|\mathbf{r}_2\|^3}\right)
\end{aligned} \tag{68}$$

where

$$\begin{aligned}
r_1 &= \sqrt{(x+\mu)^2 + y^2 + z^2} \\
r_2 &= \sqrt{(x-1+\mu)^2 + y^2 + z^2}
\end{aligned}$$

5.4. UNCERTAINTY BOUNDS

This section describes the perturbations and uncertainties that were added to the model for propagating the actual ("truth") spacecraft trajectory. These effects were not included when computing the reference halo-like orbits. The bounds on the magnitude of

these uncertainties provide guidance on how to choose the sliding mode controller parameter *F*. An exceedingly high value of this parameter will result in an excessive control signal and chattering, while a very low value will result in poor controller performance. To find an appropriate value of *F*, the known dynamic models of the following perturbation effects were analyzed to estimate bounds on them.

5.4.1. Third-Body Perturbations. Third bodies can have significant gravitational effects on the spacecraft motion depending on their mass. In this study, the gravitational effects from the solar system's largest planet Jupiter on the spacecraft is simulated and compensated for in the SMC controller. It is noted in this work that for both systems: the Sun-*433 Eros* and Sun-*4 Vesta*, the acceleration magnitude due to Jupiter is greater in magnitude than the acceleration imparted to the spacecraft due to the two primaries, namely the Sun and the small body. As a result, high station-keeping costs to maintain the spacecraft on the reference orbits that are computed neglecting Jupiter's effects are expected in these systems. To compute Jupiter's position, its heliocentric orbit is simulated assuming its orbital parameters as

$$\mu = 126.687 \times 10^6 \ \text{km}^3/\text{s}^2$$
$$a = 5.204 \ \text{AU}$$
$$e = 0.04838624$$
$$i = 1.304^o$$

where μ, a, e, i are the gravitational parameter, semimajor axis, eccentricity and inclination of Jupiter's orbit respectively. The argument of periapsis and right ascension of the ascending node (RAAN) are taken as zero. It was assumed that Jupiter is at

perijove at the start of the simulation. Jupiter's position is computed by propagating the mean-anomaly with time and then expressing the position vector in terms of the LP-centric synodic frame, from which its gravitational acceleration on the spacecraft in its reference orbit is then computed. It was observed that for the chosen reference orbits for the Sun-*433 Eros* and the Sun-*4 Vesta* systems, the gravitational acceleration was bounded in both systems along all three directions by

$$\left\|\mathbf{a}_{Jupiter}\right\| < 10^{-6} \text{ m/s}^2$$

To ensure stability, the η parameter corresponding to the discontinuous control component of the SMC controller must have a value greater than the upper bound of the perturbation given by the above in-equality. Figure 5.3 and Figure 5.4 show the acceleration due to Jupiter in the synodic frame for the Sun-*433 Eros* and the Sun-*4 Vesta* systems along the reference (nominal) as well as the actual orbit followed by the spacecraft using the SMC controller. It is noted that the Jupiter effects were only added to the dynamic model used to propagate the actual spacecraft orbit in presence of uncertainties and applied control and *not* for computing the reference orbit. The peaks in acceleration magnitude in the *x* and *y* directions for the reference orbit are due to the closeness of Jupiter to the small body during that time. The time period of the heliocentric orbit of *433 Eros* is two Earth years which is also the time duration between the peaks in the *x* direction as seen in Figure 5.3. It is noted that Jupiter only moves by a small amount during two years as its orbital period is approximately twelve years. For the Sun-*4 Vesta* system, the peaks appear every five years approximately, which is little more

than the time period of the *4 Vesta* orbit of 3.7 Earth years approximately due to Jupiter's motion.

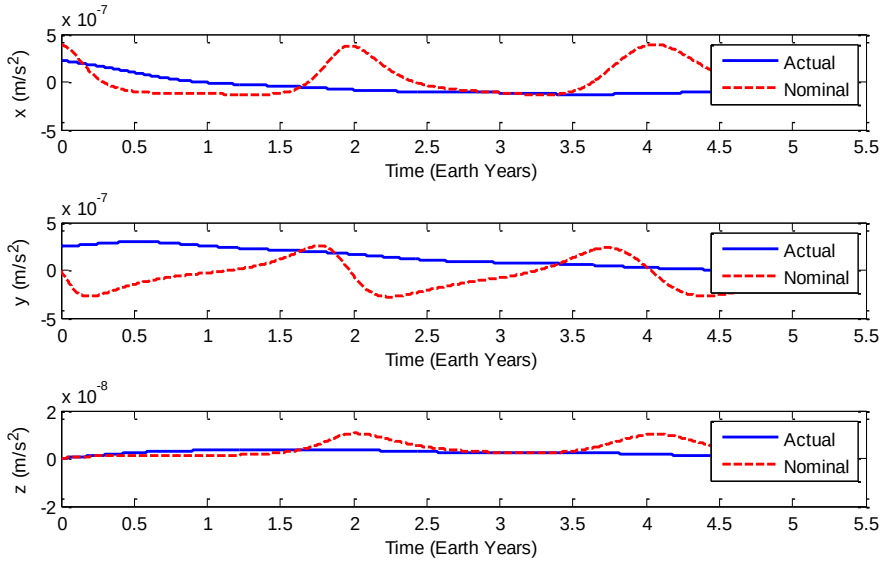

Figure 5.3. Spacecraft Acceleration due to Jupiter in the LP-Centric Synodic Frame for the Sun-*433 Eros* System.

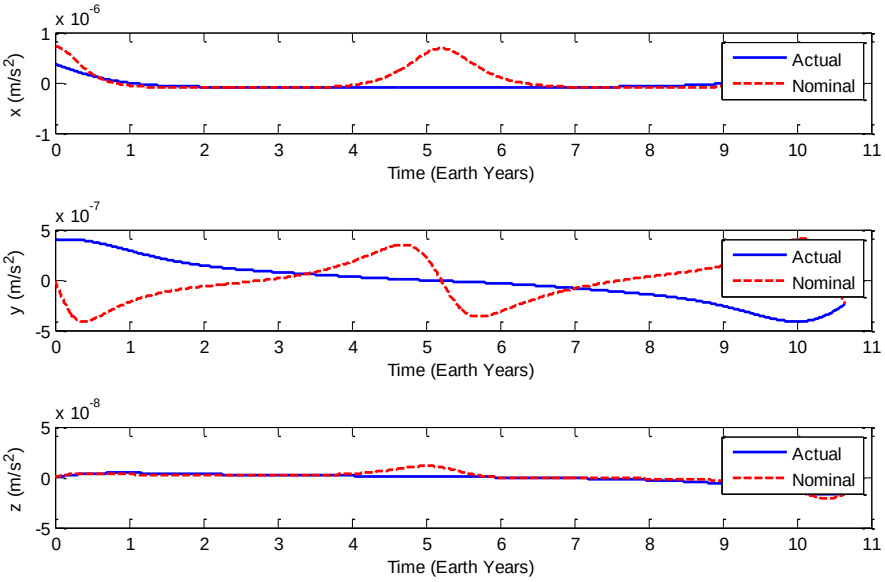

Figure 5.4. Spacecraft Acceleration due to Jupiter in the LP-Centric Synodic Frame for the Sun-*4 Vesta* System.

5.4.2. Solar Radiation Pressure. The magnitude of the solar radiation pressure (SRP) effects on the spacecraft motion depends on the spacecraft mass, size, surface material properties and distance from the Sun. In this work, the physical properties of the Orion spacecraft being developed by NASA are used[3]. The Orion mass is taken as 22,157 kg and surface area is taken as 17.35 m^2. The expression for computing SRP acceleration is given as [40]

$$\mathbf{a}_{SRP} = -\frac{\rho_{SRP} C_r A(1AU)}{m} \frac{\mathbf{r}_\odot - \mathbf{r}}{\left\|\mathbf{r}_\odot - \mathbf{r}\right\|^2} \tag{69}$$

where ρ_{SRP} is the pressure exerted by the solar radiation, C_r is the reflection coefficient of the spacecraft material, A is the spacecraft surface area normal to the incoming radiation, m is the spacecraft mass, $\mathbf{r}_\odot$ is the Sun position vector in the LP-centric synodic frame and $\mathbf{r}$ is the spacecraft position vector in the LP-centric synodic frame. To find the maximum bound on the SRP effects, the SRP acceleration was computed along the nominal libration point orbit using the maximum value of the radiation coefficient. The radiation coefficient value lies between 1.0 for translucent and 2.0 for a perfect blackbody. Typical values for the other parameters are arbitrarily assumed as

$$\begin{aligned} \rho_{SRP} &= 4.57 \times 10^{-6}\, Nm^{-2} \\ C_r &= 1.8 \end{aligned} \tag{70}$$

[3] http://www.nasa.gov/sites/default/files/617408main_fs_2011-12-058-jsc_orion_quickfacts.pdf

Figure 5.5 and 5.6 show the SRP acceleration on the Orion spacecraft in the reference halo-like orbit in the Sun-*433 Eros* and the Sun-*4 Vesta* systems respectively. The SRP acceleration along the actual orbit followed by the spacecraft using the SMC is also shown in the plots and as shown it is very close to the former case. The maximum bound for the SRP acceleration can be chosen using these plots as

$$\begin{aligned} \left\|\mathbf{a}_{SRP}\right\| &< 10^{-11} \text{ m/s}^2, \text{ Sun-433 Eros} \\ \left\|\mathbf{a}_{SRP}\right\| &< 10^{-12} \text{ m/s}^2, \text{ Sun-4 Vesta} \end{aligned} \tag{71}$$

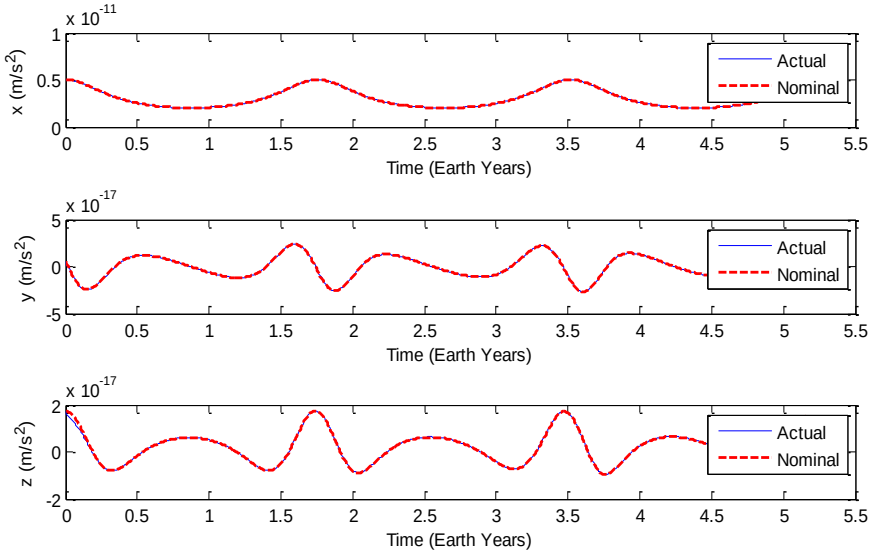

Figure 5.5. Spacecraft Acceleration due to SRP in the LP-Centric Synodic Frame for the Sun-*433 Eros* System.

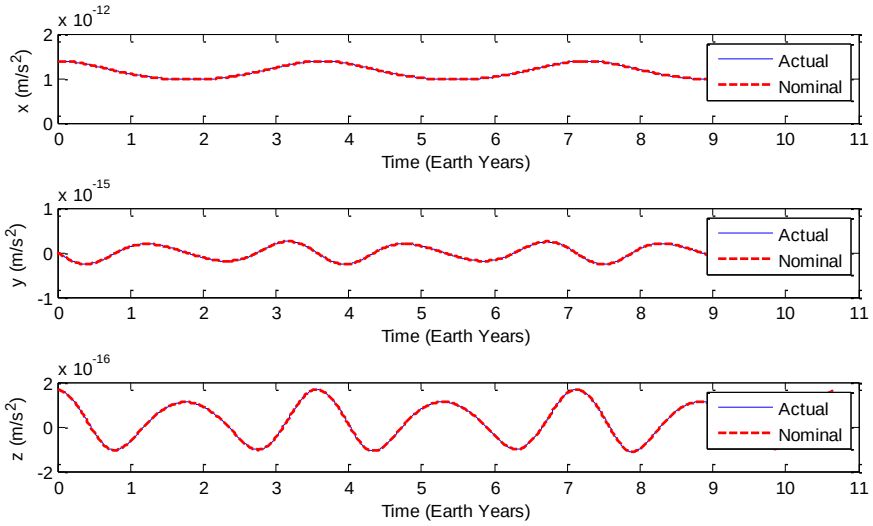

Figure 5.6. Spacecraft Acceleration due to SRP in the LP-Centric Synodic Frame for the Sun-*4 Vesta* System.

5.4.3. Tracking Errors. The sliding mode control formulation requires the knowledge of the current position and velocity of the spacecraft. Generally the current states are estimated using a filtering algorithm such as the Extended Kalman Filter that processes the sensor measurements and provides state estimates. To simulate the output of an EKF-like estimation algorithm, random time-correlated or colored noise was added to the true current states of the spacecraft before being used for computing the control. The colored noise is chosen because the estimation algorithms produce state estimates that are highly correlated in time. Reference [41] gives an algorithm for computing colored noise from given covariance values. The tracking noise standard deviation values used in this work were assumed as 1 km for position and 1 cm/s for the velocity of the spacecraft.

5.4.4. Orbit Insertion Errors. To simulate the orbit insertion errors, the initial conditions for propagating the spacecraft states are perturbed from the nominal values used in the reference orbits. For the Sun-*433 Eros* and the Sun-*4 Vesta* systems, the initial conditions were perturbed by adding random noise with position covariance of 10 km and velocity covariance of 0.1 m/s.

5.4.5. Maneuver Burn Errors. Similar to impulsive burn maneuvers, finite-burns are also affected by random inaccuracies in their execution. In this work, thruster burns (i.e. applied control accelerations) were assumed to incur 1% of colored noise, based on a rough estimate of what is expected from low-thrust propulsion systems. (some prior works in the literature use 2-3% for impulsive burns, suggesting that 1% is an appropriate value for a low-thrust system that is expected to perform with better precision).

5.5. RESULTS

In this section the simulation results for station-keeping halo-like orbits near small bodies using sliding mode control (SMC) are presented. The SMC is used for station-keeping halo-like reference orbits in two systems: Sun-*433 Eros* and Sun-*4 Vesta*. The truth trajectory was propagated with a model incorporating the effects due to the third body perturbation from Jupiter, SRP, tracking errors, orbit insertion errors and maneuver burn errors. The *MATLAB* ode113 integrator is used to integrate orbits for both systems with the relative tolerance taken as 10^{-11}. Station-keeping is simulated for a spacecraft with similar properties as the Orion spacecraft using the SMC for three revolutions of the

halo-like reference orbit, which is equivalent to six revolutions (i.e. periods) of the initial halo orbit solution in the CR3BP. In contrast to the model used to propagate the actual spacecraft trajectory, the SMC used only the nominal ER3BP dynamics for computation of the station-keeping control accelerations. For the Sun-*433 Eros* as well as the Sun-*4 Vesta* system, the third body perturbation from Jupiter is found to be the most significant perturbation. In order to compensate for the perturbations and uncertainties as seen in the previous section, the discontinuous control term of the SMC expression given in Eq. (67) must have magnitude greater than the total uncertainty expected. In other words, the η parameter is chosen such that its value is greater than the maximum perturbation accelerations expected along each direction. This parameter affects the time taken by the controller to reach the sliding surface from an initial state. Once the system reaches the sliding surface, the station-keeping error will converge to zero with a rate decided by the parameter *a* as shown in Eq. (66). In this work the following values of these parameters were chosen to keep the position error within 20 km without incurring excessive ΔV costs;

$$a = \left[10, 10, 10\right]^T \quad \eta = \left[2\times10^{-4},\, 2\times10^{-4}, 10^{-5}\right]^T \quad \text{Sun-433 Eros System}$$

$$a = \left[100, 100, 100\right]^T \quad \eta = \left[8\times10^{-4},\, 6\times10^{-4}, 3\times10^{-5}\right]^T \quad \text{Sun-4 Vesta System}$$

It was observed that without Jupiter effects, the required station-keeping cost were significantly lower. To avoid excessive station-keeping costs due to chattering in the controller, the *sign* function in Eq. (67) is replaced by a *saturation* function, which is defined as

$$sat\left(\frac{s_i}{\varepsilon}\right)=\begin{cases}\left(\frac{s_i}{\varepsilon}\right), & \left|\frac{s_i}{\varepsilon}\right|\le 1\\ sign\left(\frac{s_i}{\varepsilon}\right), & \left|\frac{s_i}{\varepsilon}\right|>1\end{cases} \tag{72}$$

where s_i is the sliding surface as defined in Eq. (66) and ε is the boundary layer around the sliding surface below which the *saturation* function varies continuously as per the above definition. The large value of the bound ε decreases the station-keeping costs but increases the station-keeping position error. Therefore a trade-off is needed in choosing its value. The following values for this bound were chosen in this work to keep the station-keeping costs low without sacrificing position accuracy despite the presence of significant uncertainties-

$$\varepsilon=[100,100,100]\text{km},\ \text{Sun-433 Eros System}$$
$$\varepsilon=[200,200,200]\text{km},\ \text{Sun-4 Vesta System}$$

Figure 5.7 shows the position error for the SMC-based station-keeping of an L_2 halo-like orbit in LP-centric synodic frame for the Sun-*433 Eros* system with eccentricity 0.2259. The maximum position error along any direction is 20 km during the simulation time of 5.17 Earth years. The control acceleration along each direction and sliding surface plot with chosen boundary layer to avoid chattering is shown in Figure 5.8 and Figure **5.9**. The total ΔV consumption for the complete simulation is found to be 125 m/s or approximately 24.5 m/s/year as shown in Figure 5.10. The maximum control acceleration

needed is $6x10^{-7}$ m/s^2, which is equivalent to 13 mN for an Orion spacecraft mass of 22,157 kg. The thrust value of 13 mN is easily achievable with current ion-propulsion systems. The xenon ion thrusters used with the Dawn mission provide 90 mN of thrust.[4] An additional benefit of ion-propulsion is that the thrusters can be throttled when required.

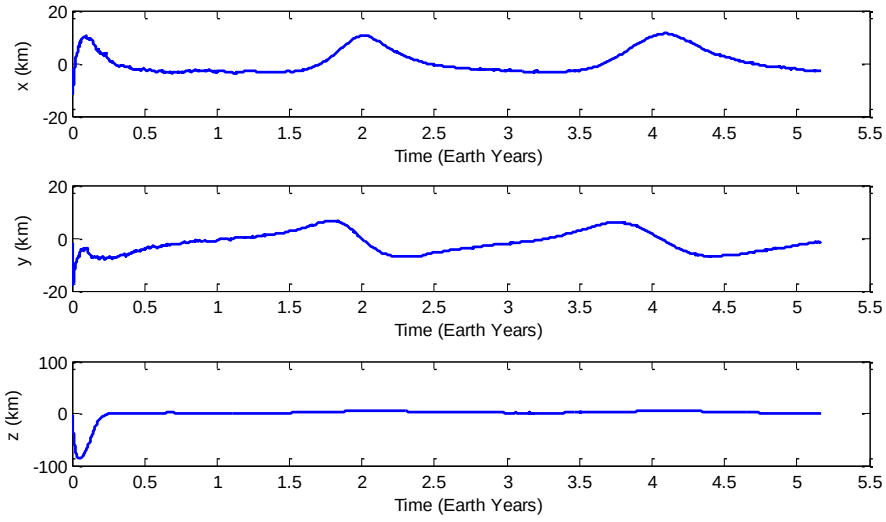

Figure 5.7. Station-Keeping Position Error in the Sun-*433 Eros* System.

[4] http://dawn.jpl.nasa.gov/mission/ion_prop.asp

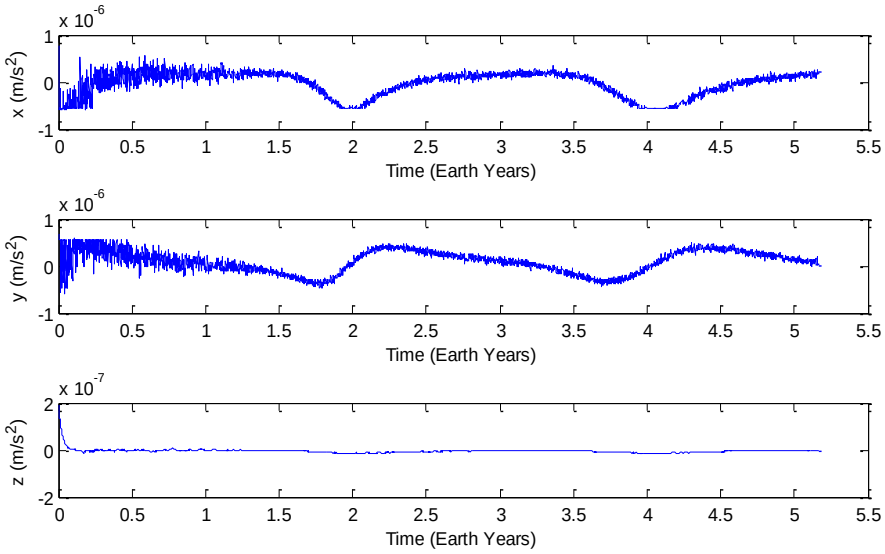

Figure 5.8. SMC Control Accelerations w.r.t. Synodic Coordinate Frame for the Sun-*433 Eros* System.

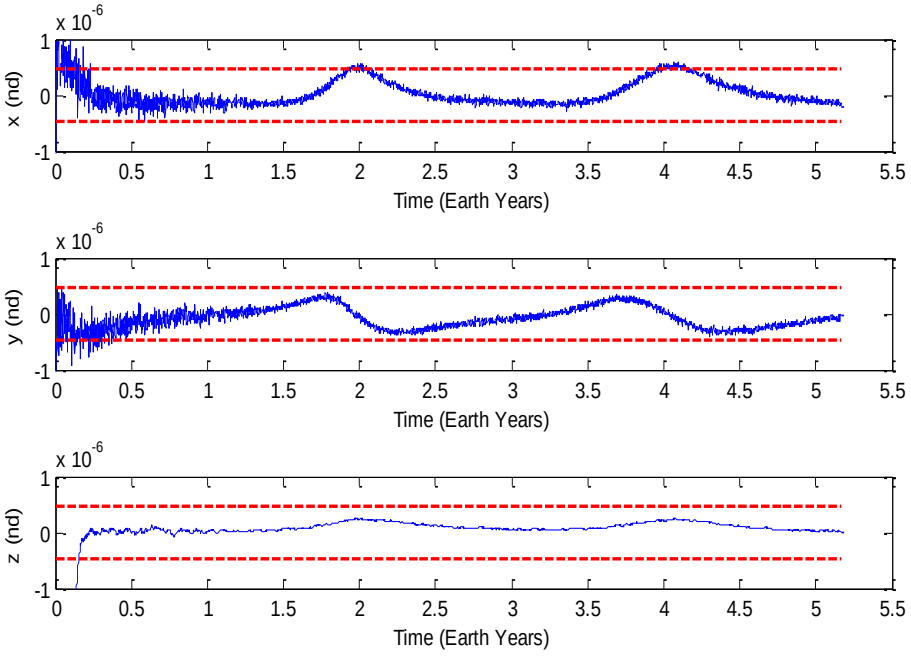

Figure 5.9. Sliding Surface "s" Along with Boundary Layer in Nondimensional Units for the Sun-*433 Eros* System.

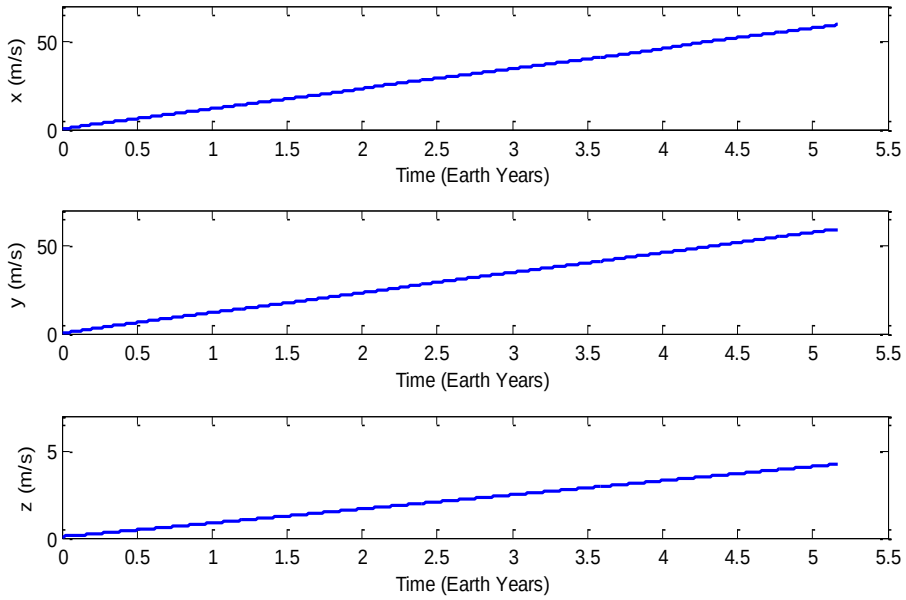

Figure 5.10. Station-Keeping ΔV for the L_2 Halo-like Orbit in the Sun-*433 Eros* System.

Similar to the Sun-*433 Eros* system, the SMC was used to station-keep a spacecraft in an L_1 halo-like orbit in the Sun-*4 Vesta* ER3BP system with eccentricity 0.0859. The three revolutions (periods) of the reference halo-like orbit are chosen that span a total of ten and a half Earth years approximately. Figure 5.11 shows the station-keeping position error, which is less than 10 km along any direction. Figure 5.12 and Figure **5.1**3 show the control acceleration applied and the corresponding sliding surface plot with the boundary layer shown. The total ΔV cost for the entire mission duration is shown in Figure 5.14 and it is found to be 417 m/s or 40 m/s/year. The maximum thrust requirement is 22 mN for the Orion spacecraft mass.

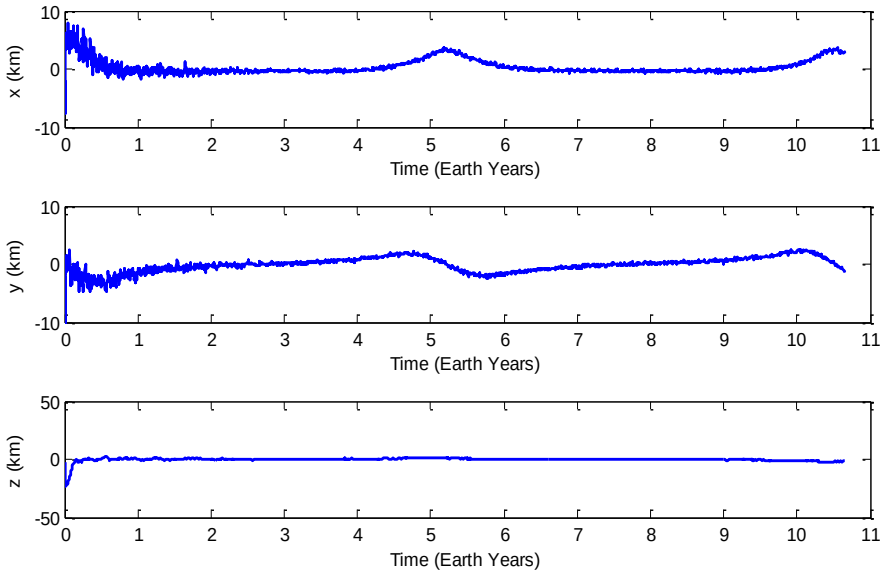

Figure 5.11. Station-Keeping Position Error in the Sun-*4 Vesta* System.

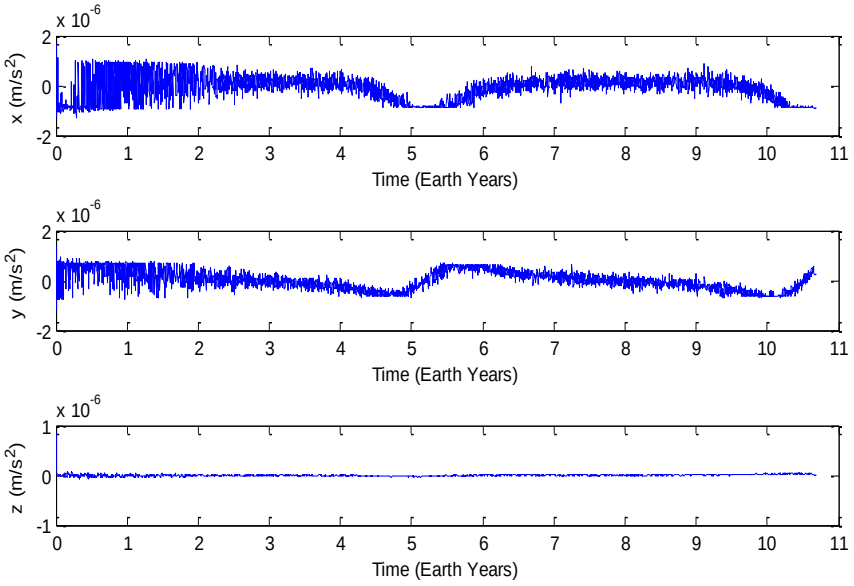

Figure 5.12. SMC Control Accelerations w.r.t. Synodic Coordinate Frame for the Sun-*4 Vesta* System.

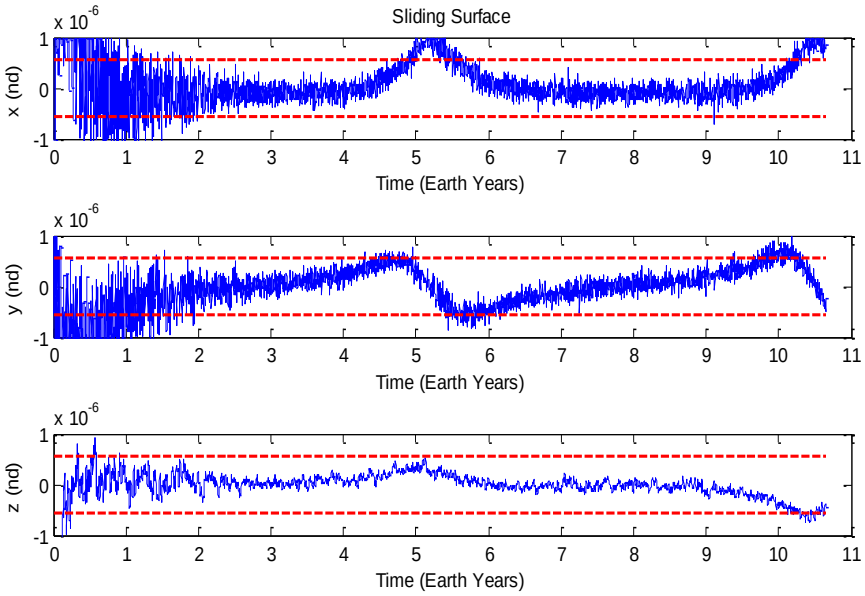

Figure 5.13. Sliding Surface "s" Along with Boundary Layer in Nondimensional Units in the Sun-*4 Vesta* System.

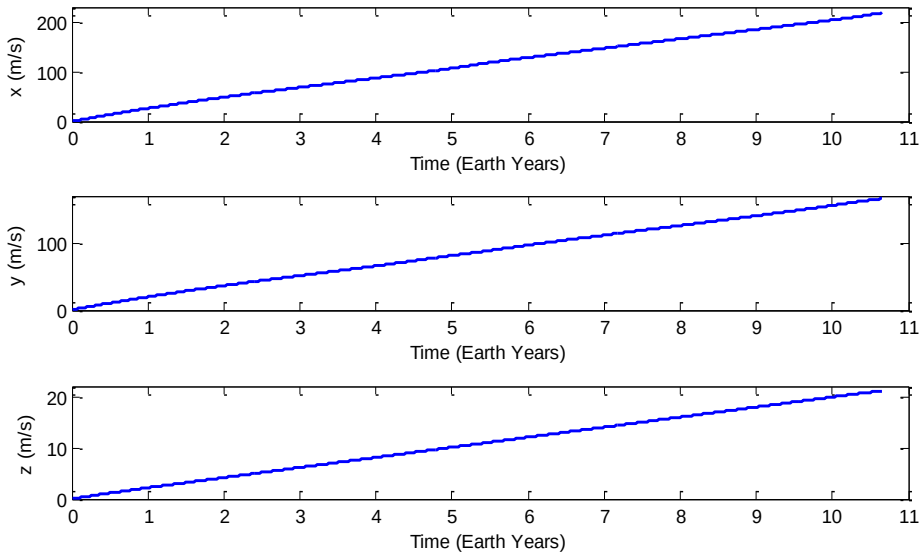

Figure 5.14. Station-Keeping ΔV for the L_1 Halo-like Orbit in the Sun-*4 Vesta* System.

6. CONCLUSION

6.1. SMALL BODY MISSIONS USING LIBRATION POINT ORBITS

Future missions to small bodies will demand more robust and accurate methods that can perform without fail in uncertain environments. In this work a novel small body mission appraoch is investigated that makes use of libration point orbits. It is shown that libration point orbits such as halo-like orbits are feasible for missions to small solar system bodies with extremely small mass ratios and eccentric heliocentric orbits. A generalized two-level differential corrector algorithm along with periodicity constraints is shown to be capable of computing halo-like orbits in the Sun-small body system. The computed halo-like orbits have a single velocity discontinuity; however it was shown that it can be avoided by choosing a reference orbit consisting of multiple revolutions in the station-keeping controller. This method has an advantage over the method employed by Broucke [9] and Campagnola *et al.* [19] in that any libration point orbit computed in the lower fidelity CR3BP model based on the mission requirements can be continued into the higher fidelity ER3BP for values of eccentricities typical of small solar system bodies. Broucke's method, which employs Moulton's strong periodicity criterion, does not have this flexibility and very few periodic solutions in the CR3BP can be continued into the ER3BP. Although only halo-like orbits were explicitly computed in this work in the ER3BP, other classes of libration point orbits such as Lissajous orbits and vertical and horizontal Lyapunov orbits can also be more easily computed using the same method. The stability analysis of the halo-like orbits computed in the vicinity of the small bodies showed that the orbits retain many characteristics typical of halo orbits such as two pairs

of stable eigenvalues and a pair of unstable eigenvalues of the monodromy matrix. It was found that with eccentricity the extent of instability increased as expected.

In addition to the method for computing reference halo-like orbits near small bodies, a station-keeping algorithm using sliding mode control theory was presented. The proposed nonlinear SMC controller was shown to be robust with regards to the perturbations from Jupiter, tracking errors, SRP perturbations, orbit insertion errors and maneuver burn errors. The nonlinear controller assumed continuous low-thrust control and provided "tight" control with position error less than 20 km for both cases considered: halo-like orbits in the Sun-*433 Eros* and Sun-*4 Vesta* systems. The associated station-keeping costs found to be of the order of 30-40 m/s/year. Although these values are a higher than existing methods [27], [29], [30], the proposed station-keeping controller provides "tight" control despite the presence of significant uncertainties. The SMC is, by design, better suited in uncertain environments with structured and unstructured uncertainties.

6.2. FUTURE WORK

The reference halo-like orbits near small bodies in this work were computed in the ER3BP. Pernicka has shown that this method can also be utilized to find Lissajous orbits in a Sun-Earth-Moon ephemeris-based model [21]. The proposed differential corrector, along with periodicity constraints, can be validated against an ephemeris-based model. When used in the station-keeping algorithm, the resulting orbits computed in the ephemeris model will likely reduce the station-keeping costs further.

The SMC station-keeping controller can also be validated with the higher fidelity ephemeris model. It was seen that the SMC controller was not very efficient in correcting the orbit insertion errors. More work is needed for mitigating the orbit insertion errors without incurring high station-keeping costs.

BIBLIOGRAPHY

[1] N. R. Augustine, W. M. Austin, C. Chyba, C. F. Kennel, and E. Al., "Seeking a Human Spaceflight Program Worthy of a Great Nation," 2009.

[2] V. Szebehely, "Theory of Orbits: The Restricted Problem of Three Bodies," *Astrophysics and Space Science*, 1967.

[3] W. S. Koon, M. W. Lo, J. E. Marsden, and S. D. Ross, *Dynamical Systems, The Three-Body Problem, and Space Mission Design*. Springer-Verlag, New York, 2006.

[4] H. C. Plummer, "On Oscillating Satellites," *Monthly Notices of the Royal Astronomical Society*, Vol. 63, No. 436, 1903.

[5] J. M. A. Danby, "Stability of the Triangular Points in the Elliptic Restricted Problem of Three Bodies," *The Astronomical Journal*, Vol. 69, No. 2, 1964, pp. 165–172.

[6] A. Bennett, "Characteristic Exponents of the Five Equilibrium Solutions in the Elliptically Restricted Problem," *Icarus*, Vol. 4, 1965, pp. 177–187.

[7] K. T. Alfriend and R. H. Rand, "Stability of the Triangular Points in the Elliptic Restricted Problem of Three Bodies," *AIAA Journal*, Vol. 7, No. 6, 1969.

[8] A. Bennett, "Analytical Determination of Characteristic Exponents," *Methods in Astrodynamics and Celestial Mechanics*, Vol. 17, p. 101, 1966.

[9] R. Broucke, "Stability of Periodic Orbits in the Elliptic, Restricted Three-Body Problem.," *AIAA Journal*, Vol. 7, No. 6, pp. 1003–1009, Jun. 1969.

[10] P. E. Schmid, "Lunar Far-Side Communication Satellites," 1968.

[11] R. W. Farquhar, "Lunar Communication with Libration-Point Satellites," *Journal of Spacecraft and Rockets*, Vol. 4, 1967, pp. 1383–1384.

[12] R. W. Farquhar and A. A. Kamel, "Quasi-Periodic Orbits About the Translunar Libration Point," *Celestial Mechanics*, Vol. 7, 1973, pp. 458–473.

[13] T. A. Heppenheimer, "Out-Of-Plane Motion About Libration Points: Nonlinearity and Eccentricity Effects," *Celestial Mechanics*, Vol. 7, No. 2, 1973, pp. 177–194.

[14] D. L. Richardson and N. D. Cary, "A Uniformly Valid Solution for Motion about the Interior Libration Point of the Perturbed Elliptic-Restricted Problem," in *AAS/AIAA Astrodynamics Specialist Conference*, 1975.

[15] D. L. Richardson, "Analytic Construction of Periodic Orbits About the Collinear Points," *Celestial Mechanics*, Vol. 22, 1980, pp. 241–253.

[16] G. Gomez, J. Masdemont, and C. Simo, "Quasihalo Orbits Associated With Libration Points," 1982, pp. 7–8.

[17] K. C. Howell, "Three-Dimensional, Periodic,'Halo' Orbits," *Celestial Mechanics*, Vol. 32, 1984, pp. 53–71.

[18] K. C. Howell, "Three-Dimensional Periodic Halo Orbits In the Restricted Three-Body Problem," Ph.D. Dissertation, Stanford University, 1983.

[19] S. Campagnola and M. Lo, "Subregions of Motion and Elliptic Halo Orbits in the Elliptic Restricted Three-Body Problem," in *AAS/AIAA Spaceflight Mechanics*, 2008.

[20] K. Howell and H. Pernicka, "Numerical Determination of Lissajous Trajectories in the Restricted Three-Body Problem," *Celestial Mechanics and Dynamical Astronomy*, 1987.

[21] H. Pernicka, "The Numerical Determination of Nominal Libration Point Trajectories and Development of a Station-Keeping Strategy," Ph.D. Dissertation, Purdue University, 1990.

[22] B. G. Marchand, K. C. Howell, and R. S. Wilson, "An Improved Corrections Process for Constrained Trajectory Design in the n-Body Problem," *Journal of Spacecraft and Rockets*, Vol. 44, No. 4, Jul. 2007, pp. 884–897.

[23] X. Y. Hou and L. Liu, "On Motions Around the Collinear Libration Points in the Elliptic Restricted Three-Body Problem," *Monthly Notices of the Royal Astronomical Society*, Vol. 415, No. 4, Aug. 2011, pp. 3552–3560.

[24] D. Scheeres and F. Marzari, "Spacecraft Dynamics in the Vicinity of a Comet," *Journal of the Astronautical Sciences*, Vol. 50, No. 1, pp. 35–52, 2002.

[25] R. W. Farquhar, "The Utilization of Halo Orbits in Advanced Lunar Operations," Report, 1971.

[26] J. V. Breakwell, A. A. Kamel, and M. J. Ratner, "Station-Keeping for a Translunar Communication Station," *Celestial Mechanics*, Vol. 10, 1974, pp. 357–373.

[27] K. C. Howell and H. J. Pernicka, "Stationkeeping Method for Libration Point Trajectories," *Journal of Guidance, Control, and Dynamics,* Vol. 16, No. 1, 1993, pp. 151–159.

[28] K. Williams, B. Barden, K. Howell, M. Lo, and R. Wilson, "Genesis Halo Orbit Station Keeping Design," 2000.

[29] D. Cielaszyk and B. Wie, "New Approach to Halo Orbit Determination and Control," *Journal of Guidance, Control, and Dynamics,* Vol. 19, No. 2, Mar. 1996, pp. 266–273.

[30] P. Gurfil and D. Meltzer, "Stationkeeping on Unstable Orbits: Generalization to the Elliptic Restricted Three-Body Problem," *Journal of the Astronautical Sciences,* Vol. 54, No. 1, 2006, pp. 1–23.

[31] G. Gomez, K. Howell, J. Masdemont, and C. Simo, "Station-Keeping Strategies for Translunar Libration Point Orbits," in *AAS,* 1998, pp. 1–20.

[32] D. Folta and F. Vaughn, "A Survey of Earth-Moon Libration Orbits : Stationkeeping Strategies And Intra-Orbit Transfers," in *AIAA/AAS Astrodynamics Specialist Conference and Exhibit,* August 2004.

[33] J. Kulkarni, M. E. Campbell, and G. E. Dullerud, "Stabilization of Spacecraft Flight in Halo Orbits: An H_∞ Approach," *IEEE Transactions on Control System Technology,* Vol. 14, No. 3, 2006, pp. 572–578.

[34] N. Lincoln and S. Veres, "Six Degree of Freedom Variable Hierarchy Sliding Mode Control in Halo Orbits with Potential Function Guidance," in *47th IEEE Conference on Decision and Control,* 2008.

[35] D. C. Folta, T. A. Pavlak, K. C. Howell, M. A. Woodard, and D. W. Woodfork, "Stationkeeping of Lissajous Trajectories in the Earth-Moon System with Applications to ARTEMIS," in *AAS Paper,* 2010.

[36] T. Pavlak and K. Howell, "Strategy for Long-Term Libration Point Orbit Stationkeeping in the Earth-Moon System," in *AAS,* 2011.

[37] C. Chen, *Linear System Theory and Design*, 2nd Edition, Oxford University Press, USA, 1995.

[38] J.-J. E. Slotine and W. Li, *Applied Nonlinear Control*. Prentice Hall, Inc., 1991.

[39] H. Khalil, *Nonlinear Systems,* 3rd Edition, Prentice Hall, Inc., 2001.

[40] D. A. Vallado, *Fundamentals of Astrodynamics and Applications*. Microcosm, Inc, 2001.

[41] D. Simon, *Optimal State Estimation*. John Wiley & Sons, Inc., New Jersey, 2006.

VITA

Bharat Mahajan was born in 1984 in New Delhi, India. He graduated from S. M. Jain Hr. Sc. School, Jammu in March 2001 and received his Bachelor of Engineering in Electronics and Communication degree from The University of Jammu in July 2007. After undergraduate studies, he worked as a System Software Engineer in Hewlett-Packard, India for three years. Bharat began his graduate studies at Missouri University of Science and Technology, Rolla in August 2010. He worked as a Research Intern in IST-Rolla from July 2012 to December 2012 and received his Master of Science in Aerospace Engineering degree in December 2013. Bharat is a student member of AIAA and AAS.